



저작자표시 2.0 대한민국

이용자는 아래의 조건을 따르는 경우에 한하여 자유롭게

- 이 저작물을 복제, 배포, 전송, 전시, 공연 및 방송할 수 있습니다.
- 이차적 저작물을 작성할 수 있습니다.
- 이 저작물을 영리 목적으로 이용할 수 있습니다.

다음과 같은 조건을 따라야 합니다:



저작자표시. 귀하는 원저작자를 표시하여야 합니다.

- 귀하는, 이 저작물의 재이용이나 배포의 경우, 이 저작물에 적용된 이용허락조건을 명확하게 나타내어야 합니다.
- 저작권자로부터 별도의 허가를 받으면 이러한 조건들은 적용되지 않습니다.

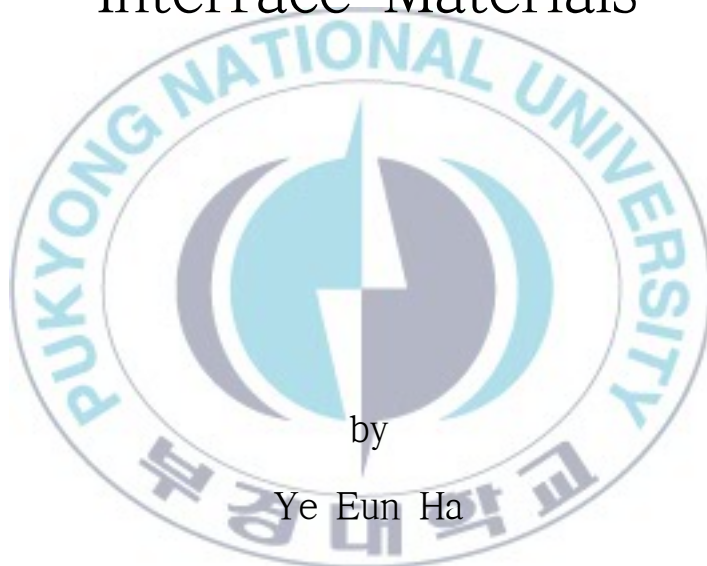
저작권법에 따른 이용자의 권리는 위의 내용에 의하여 영향을 받지 않습니다.

이것은 [이용허락규약\(Legal Code\)](#)을 이해하기 쉽게 요약한 것입니다.

[Disclaimer](#) 

Thesis for the Degree of Master of Engineering

Polymer Solar Cells and Light-Emitting Diodes with Cathode Interface Materials



by

Ye Eun Ha

Department of Polymer Engineering

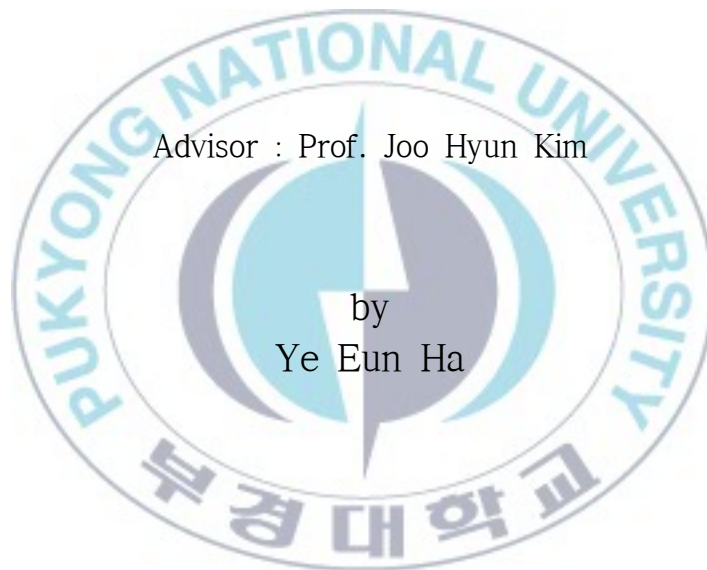
The Graduate School

Pukyong National University

February 2014

Polymer Solar Cells and Light-Emitting
Diodes with Cathode Interface
Materials

(음극 층간 물질을 가진 고분자
태양전지 및 발광소자)



A thesis submitted in partial fulfillment of the requirements
For the degree of

Master of Engineering

in Department of Polymer Engineering, The Graduate School,
Pukyong National University

February 2014
Polymer Solar Cells and Light-Emitting Diodes
with Cathode Interface Materials

A dissertation
by
Ye Eun Ha

Approved by :

(Chairman) Prof. Bong Lee

(member) Prof. Seong-II Yoo

(member) Prof. Joo Hyun Kim

February 21, 2014

Contents

Contents..... I

List of Figures..... VI

List of Tables XI

List of Schemes..... XII

Abstract XIII

Chapter I. Introduction

I-1. Structure and Basic Principles of Devices

 I-1-1. Conventional Type Polymer Solar Cells 1

 I-1-2. Inverted Type Polymer Solar Cells 4

 I-1-3. Polymer Light Emitting Diodes 6

I-2. Parameters of Devices

 I-2-1. Parameters of Polymer Solar Cells..... 8

 I-2-2. Parameters of Polymer Light-Emitting Diodes 11

I-3. Self-Assembled Monolayers 12

I-4. Measurement 13

Chapter II. Inverted type Polymer Solar Cells Using Self-Assembled Monolayer treated ZnO with Benzoyl Chloride Derivatives as Electron Transporting Materials

II-1. Introduction.....	15
II-2. Experiment Section	
II-2-1. Materials.....	17
II-2-2. Fabrication of IPSCs.....	18
II-3. Results and Discussion	
II-3-1. Characterization of SAM modified ZnO.....	19
II-3-2. Photovoltaic Properties of IPSCs.....	24
II-3-3. Surface Properties of IPSCs.....	27
II-4. Conclusion.....	32

Chapter III. Inverted type Polymer Solar Cells Using Self-Assembled Monolayer treated ZnO with Benzoic Acid Derivatives as Electron Transporting Materials

III-1. Introduction	33
III-2. Experiment Section	
III-2-1. Materials.....	34
III-2-2. Fabrication of IPSCs.....	35
III-3. Results and Discussion	
III-3-1. Characterization of SAM modified ZnO.....	38
III-3-2. Photovoltaic Properties of IPSCs.....	43
III-3-3. Surface Properties of the Active Layer	49
III-4. Conclusion.....	54
 Chapter IV. Inverted type Polymer Solar Cells Using Self-Assembled Monolayer treated ZnO with Aryl Benzoic Acid Derivatives as Electron Transporting Materials	
IV-1. Introduction.....	55
IV-2. Experiment Section	
IV-2-1. Materials.....	56

IV-2-2. Synthesis of 4-(diphenylamino)benzoic acid (DPA-BA) and 4-(9H-carbazol-9-yl)benzoic acid (Cz-BA)	57
IV-2-3. Fabrication of IPSCs	62
 IV-3. Results and Discussion	
IV-3-1. Characterization of SAM modified ZnO	64
IV-3-2. Photovoltaic Properties of IPSCs	68
IV-3-3. Surface Properties of the Active Layer	73
 IV-4. Conclusion.....	76
 Chapter V. Conventional type Polymer Solar Cells and Polymer Light Emitting Diodes Using Non-conjugated Polymer with Polar Group as Electron Transporting Materials	
 V-1. Introduction.....	77
 V-2. Experiment Section	
V-2-1. Materials	78
V-2-2. Fabrication of CPSCs	79
V-2-3. Fabrication of PLEDs.....	80

V-3. Results and Discussion

V-3-1. Characterization of CPSCs and PLEDs with Poly vinyl alcohol
(PVA).....81

V-3-2. Photovoltaic Properties of CPSCs..... 83

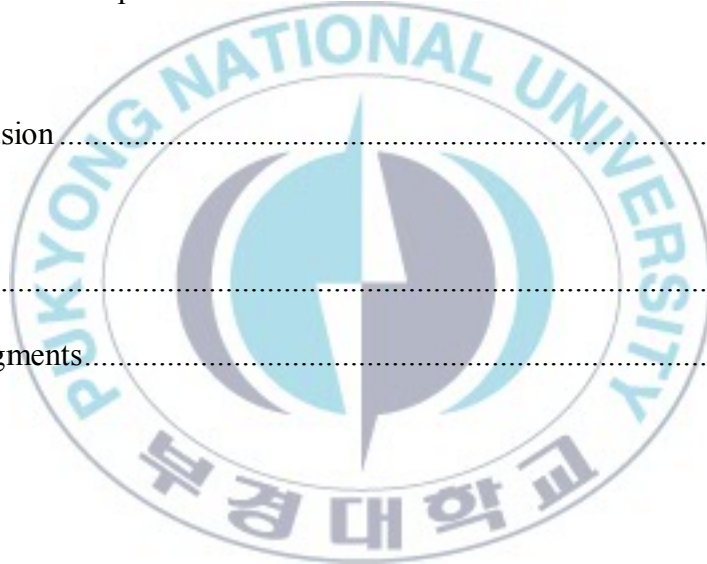
V-3-3. Luminescent Properties of PLEDs 89

V-3-4. Surface Properties of CPSCs 94

V-4. Conclusion 98

References 99

Acknowledgments..... 104



List of Figures

Figure 1-1. Typical structure of CPSC.

Figure 1-2. Operating mechanisms of PSC.

Figure 1-3. Typical structure of IPSC.

Figure 1-4. Typical structure of PLEDs.

Figure 1-5. Parameters of PSC in J-V curve.

Figure 2-1. O_{1s} XPS spectra of (a) ZnO, (b) FBC treated ZnO and (c) BBC treated ZnO.

Figure 2-2. The devices structures and the chemical structures used in the device fabrications and energy diagram of ITO/ZnO/P3HT:PCBM/WO₃/Ag device with or without SAM.

Figure 2-3. UPS spectra of ZnO, FBC coated ZnO and BBC coated ZnO.

Figure 2-4. Current density–voltage curves of PSCs (a) under AM 1.5G simulated illumination with an intensity of 100mW/cm² and (b) under the dark condition (rectangular: without SAM treatment, circle: with FBC treated from solution of 20 μ/ml and triangle: with BBC treated from solution of 20 μ/ml).

Figure 2-5. Contact angle of (a) FBC on ZnO surface, (b) ZnO surface and (c) BBC on ZnO surface (water drop on the top of ZnO, FBC and BBC).

Figure 2-6. Optical microscope images of ITO/ZnO/(FBC or BBC)/P3HT:PCBM surface. (X40).

Figure 2-7. AFM height images of thermally annealed P3HT:PCBM film on (a) ZnO/FBC (b) ZnO and (c) ZnO/BBC.

Figure 3-1. Structure of Devices and Self-Assembled Molecules.

Figure 3-2. XPS spectra of (a) ZnO, (b) ZnO/FBA, (c) ZnO/BBA and (d) ZnO/MBA.

Figure 3-3. Interfacial dipole direction between ZnO and the active layer.

Figure 3-4. Effective work function of ZnO/FBA, ZnO, ZnO/BBA and ZnO/MBA.

Figure 3-5. Current density-voltage curves of inverted type PSCs (a) under AM 1.5G simulated illumination with an intensity of 100 mW/cm^2 and (b) under the dark condition (square, FBA SAM modified; circle, without SAM; triangle, BBA SAM modified; inverted triangle, MBA SAM modified).

Figure 3-6. (a) J_{sc} , (b) V_{oc} , (c) FF, (d) PCE, (e) R_s and (f) V_{oc} vs. effective work function.

Figure 3-7. IPCE spectra of the devices ZnO/FBA, ZnO, ZnO/BBA and ZnO/MBA.

Figure 3-8. TEM images of the active layer deposited on (a) ZnO/FBA, (b) ZnO, (c) ZnO/BBA, and (d) ZnO/MBA.

Figure 3-9. AFM topography images of thermally annealed P3HT/PCBM film on

(a) ZnO/FBA, (b) ZnO, (c) ZnO/BBA, and (d) ZnO/MBA ($x, y = 1 \mu\text{m}/\text{div.}$, $z = 100 \text{ nm}/\text{div.}$).

Figure 3-10. The surface energy of ZnO/FBA, ZnO, ZnO/BBA, and ZnO/MBA.

Figure 4-1. XPS Spectra of (a) ZnO, (b) ZnO/DPA-BA and (c) ZnO/Cz-BA.

Figure 4-2. UPS spectra of ZnO, ZnO treated DPA-BA and Cz-BA.

Figure 4-3. Current density-voltage curves of inverted type PSCs (a) under AM 1.5G simulated illumination with intensity of $100 \text{ mW}/\text{cm}^2$ and (b) under the dark condition (square, ZnO; circle, DPA-BA treated ZnO; triangle, Cz-BA treated ZnO).

Figure 4-4. Schematic illustration of polymer solar cells with SAM modified ZnO and schematic energy level diagram of the devices with SAM modified ZnO. For ZnO/DPA-BA and ZnO/Cz-BA, the interfacial dipole directed away from ZnO. There is no net interfacial dipole for ZnO without SAM.

Figure 4-5. AFM topography images of thermally annealed P3HT/PCBM film on

(a) ZnO, (b) ZnO/ DPA-BA, and (c) ZnO/Cz-BA ($x, y = 1 \mu\text{m}/\text{div.}$, $z = 100 \text{ nm}/\text{div.}$).

Figure 4-6. Photographs from water contact angle measurements on (a) ZnO, (b) DPA-BA treated ZnO, and (c) Cz-BA treated ZnO.

Figure 5-1. UPS spectra of PVA treated Al and ITO.

Figure 5-2. Structure of CPSCs with PVA.

Figure 5-3. Current density-voltage curves of CPSCs (a) under AM 1.5G simulated illumination with an intensity of 100 mW/cm^2 and (b) under the dark condition.

Figure 5-4. IPCE Spectra of CPSCs with PVA in DMSO/MeOH solution.

Figure 5-5. Structure of PLEDs with PVA.

Figure 5-6. Current density-Voltage-Brightness spectra of PLEDs (a) without PVA, (b) with PVA of 0.2 mg/mL , (c) with PVA of 0.5 mg/mL and (d) with PVA of 1.0 mg/mL .

Figure 5-7. Luminance efficiency spectra of PLEDs without PVA and with PVA.

Figure 5-8. Water contact angle of films (a) without PVA, (b) with PVA of 0.2 mg/mL in $\text{H}_2\text{O/MeOH}$, (c) with PVA of 0.5 mg/mL in $\text{H}_2\text{O/MeOH}$, (d) with PVA of 0.2 mg/mL in DMSO/MeOH (e) with PVA of 0.5 mg/mL in DMSO/MeOH and (f) with PVA of 1.0 mg/mL in DMSO/MeOH.

Figure 5-9. AFM images of the device (a) without PVA, (b) with PVA of 0.2 mg/mL in $\text{H}_2\text{O/MeOH}$, (c) with PVA of 0.5 mg/mL in $\text{H}_2\text{O/MeOH}$, (d) with PVA of 0.2 mg/mL in DMSO/MeOH (e) with PVA of 0.5 mg/mL in DMSO/MeOH and (f) with PVA of 1.0 mg/mL in DMSO/MeOH.

List of Tables

Table 2-1. Photovoltaic properties of inverted solar cells treated FBC and BBC.

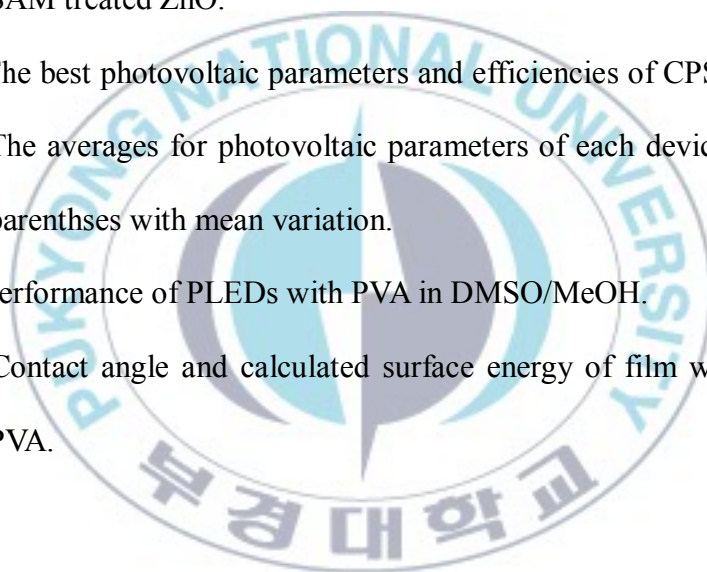
Table 3-1. The best photovoltaic parameters and efficiencies of PSC with various SAM treated ZnO. The averages for photovoltaic parameters of each device are given in parentheses with mean variation.

Table 4-1. Best photovoltaic parameters and efficiencies of PSCs with various SAM treated ZnO.

Table 5-1. The best photovoltaic parameters and efficiencies of CPSCs with PVA. The averages for photovoltaic parameters of each device are given in parentheses with mean variation.

Table 5-2. Performance of PLEDs with PVA in DMSO/MeOH.

Table 5-3. Contact angle and calculated surface energy of film without or with PVA.



List of Schemes

Scheme 4-1. Synthesis of 4-(diphenylamino)benzoic acid (DPA-BA) and 4-(9H-carbazol-9-yl)benzoic acid (Cz-BA)



음극 층간 물질을 가진 고분자태양전지 및 발광소자

하예은

부 경 대 학 교 대 학 원 고 분 자 공 학 과

요 약

최근, 고분자 태양전지(Polymer Solar Cells)와 발광 소자 (Polymer Light Emitting Diodes)와 같은 유기 광전 소자는 적은 제작비용과 유연 소자(flexible devices)에 응용가능성이 있어 각광 받고 있는 연구 분야이다. 소자 내 전자 수송 능력, 전자 주입능력은 소자의 성능에 영향을 미치는 중요한 요소이며, 이 요소들은 고분자 태양전지에서는 광활성층과 전극 사이에서, 발광소자에서는 발광층과 전극 사이에서의 층간 성질에 따라 크게 달라진다. 층간 성질을 효율적으로 조절하는 방법으로는 자기조립 단분자막 (Self-Assembled Monolayer (SAM))과 완충층 (Buffer Layer)이 많이 사용되고 있고, 이 방법들은 층간 소재의 영구쌍극자 (permanent dipole)에 의해 금속 전극의 일함수(work function)를 낮추고 층간 접촉저항을 줄여 소자의 효율을 향상시킨다. 본 연구에서는 Benzoyl chloride 유도체와 Benzoic acid 유도체를 SAM 처리하여 역구조(inverted type)의 고분자 태양전지를 제작하고, 광전기적 특성과 층간 morphology 를 연구하였다. 또한 기존의 발표된 층간 소재와 달리 비 공액 고분자인 Poly(vinyl alcohol)을 음전극의

완충층으로 사용하여 정구조의 고분자 태양전지와 발광소자를 제작하고, 광전기적 특성과 층간 특성을 연구하였다.



Chapter I. Introduction

I-1. Structure and Basic Principles of Devices

I-1-1. Conventional Polymer Solar Cells

A typical conventional polymer solar cell (CPSC) is consisting of two electrodes (anode and cathode), a photo-active layer (a blend of electron donor and acceptor) and buffer layers. Figure 1-1 shows the architecture of typical CPSC. Transparent indium tin oxide (ITO) with high work function is used as an anode, Aluminum (Al) or Calcium (Ca) with low work function is used as a cathode in CPSCs. The active layer is composed of donor (D) and acceptor (A). The hole transporting layer (HTL) is located between the anode and the active layer. On the contrary, the electron transporting layer is located between the cathode and the active layer. Recently, PSCs are fabricated by using solution process such as spin coating, ink-jet printing and screen printing.

The operating principles CPSCs show Figure 1-2. When the devices absorb a photon either by electron donor and/or electron acceptor, it lead to the formation of an excited state, that is, the bound electron-hole pairs creation (called exciton). Exciton diffuses at the interface between the electron D and the electron A, that is charge separation. Then separated charges (electrons and holes) transport to the electrodes.

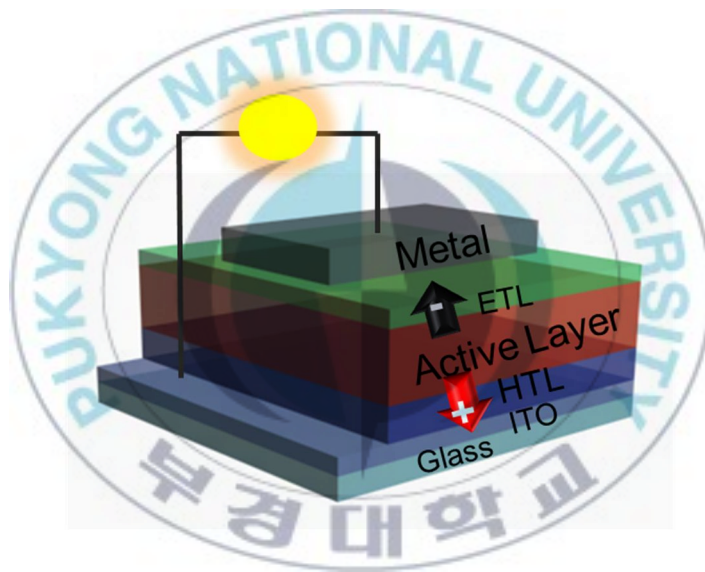


Figure 1-1. Typical structure of CPSC.

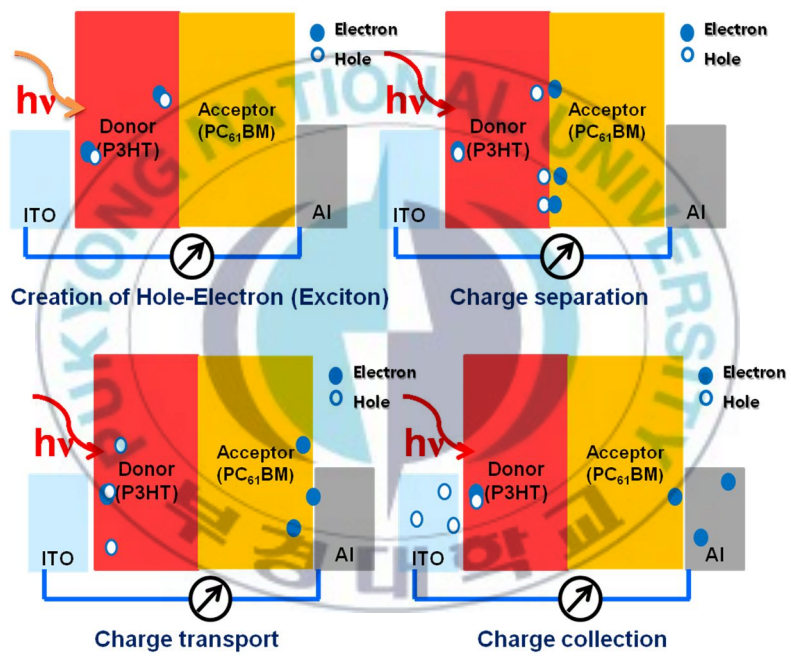
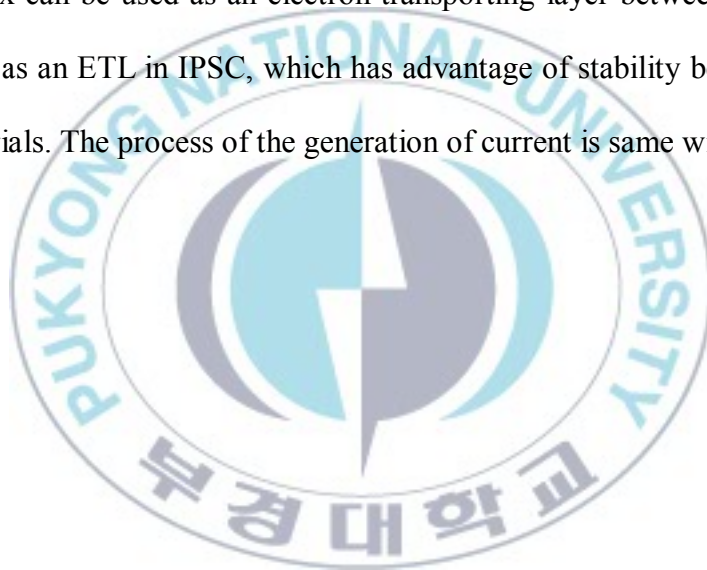


Figure 1-2. Operating mechanisms of PSC.

I-1-2. Inverted Type Polymer Solar Cells

Inverted type polymer solar cells (IPSCs) is created to improve stability of the device and is supplemented the weakness of acidic poly(3,4-ethylenedioxythiophene) poly(styrenesulfonate) (PEDOT:PSS) as a HTL in CPSCs. Usually, transparent substrate, ITO, is used as cathode, and silver (Ag) with high work function is used as anode in IPSCs. n-Type metals oxides such as ZnO or TiO_x can be used as an electron transporting layer between ITO and the active layer as an ETL in IPSC, which has advantage of stability because of non-acidic materials. The process of the generation of current is same with CPSCs.



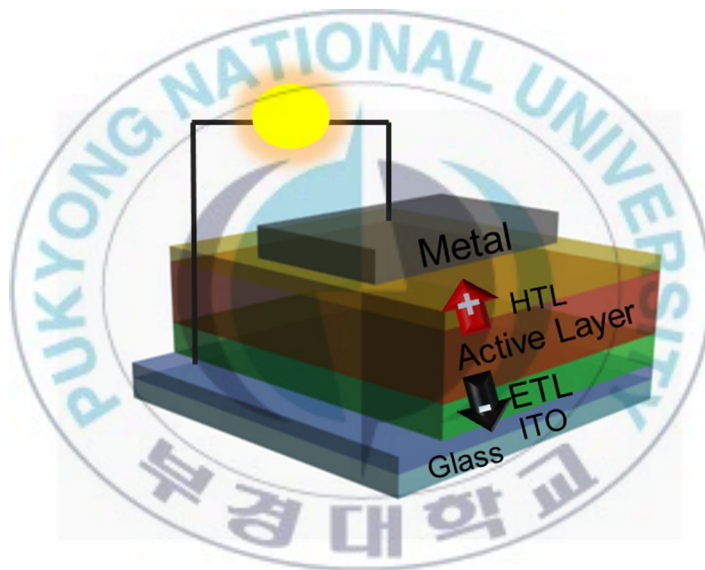
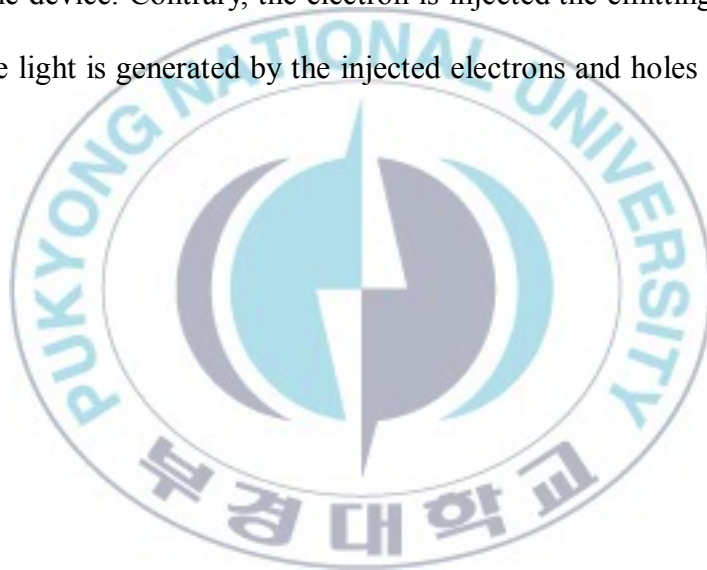


Figure 1-3. Typical structure of IPSC.

I-1-3. Polymer Light Emitting Diodes

Polymer light-emitting diodes (PLEDs) are consisted of the emitting layer between ITO and metal electrode in Figure 1-4. The buffer layer such as electron injection layer (EIL) and hole injection layer (HIL) is commonly used to fabrication of PLED to improve efficiency.

The hole is injected the emitting layer through the HIL, when the electric filed is applied to the device. Contrary, the electron is injected the emitting layer through the EIL. The light is generated by the injected electrons and holes at the emitting layer.



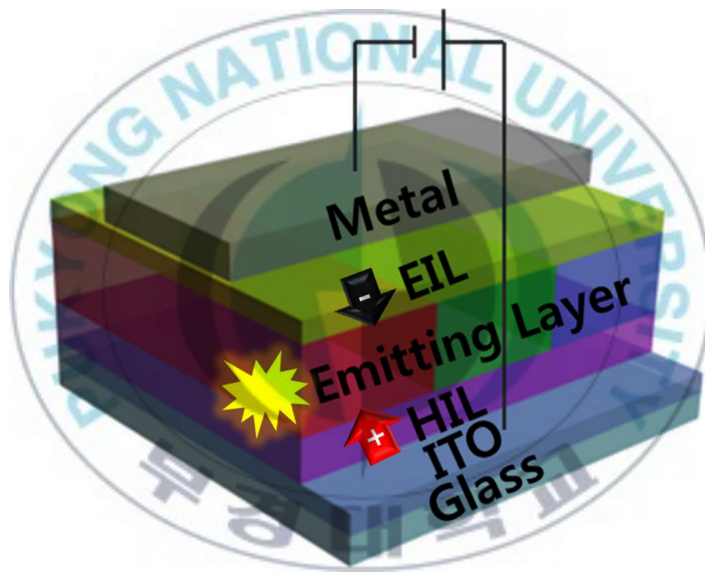


Figure 1-4. Typical structure of PLED.

I-2. Parameters of Devices

I-2-1. Parameters of Polymer Solar Cells

The short-circuit current (J_{sc}), the open circuit voltage (V_{oc}), the fill factor (FF) and the power conversion efficiency (PCE) are basic polymer solar cell (PSC) parameters. As shown Figure 1-5, J-V curves under the dark and illuminated condition. The open circuit voltage (V_{oc}) is no current flows by a polymer solar cell. At the donor-accepter interface generate ΔE between the HOMO of donor and LUMO of acceptor which is the energy difference. For $V = 0$ only J_{sc} flows through the solar cell which is purely based on photo generated charge carriers. Thus, for monochromatic exposure the spectral dependence of the charge carrier generation can be measured.

The maximum power P_{max} of a solar cell is determined by the maximum power in the J-V curve. Therefore, the fill factor (FF) is defined below,

$$FF = \frac{P_{max}}{J_{sc} V_{oc}}$$

As shown Figure 1-5, FF is given by the inner square which is an indicator of the quality of a solar cell. In PSCs, the FF indicated by the serial electrical resistance (R_s) of the cell and therefore by the charge carrier mobility.

The PCE of PSCs defined as

$$PCE = \frac{J_{sc} V_{oc} FF}{P_{in}}$$

where P_{in} is the incident light power which is standardized as 100 mW/cm^2 .



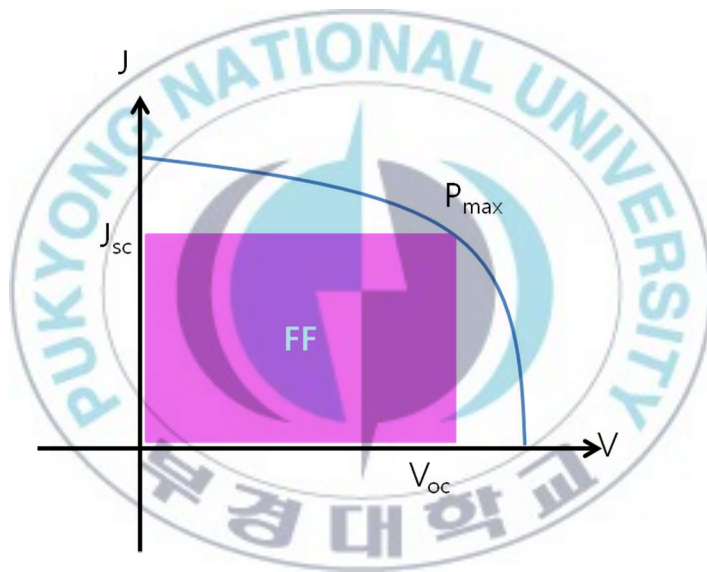


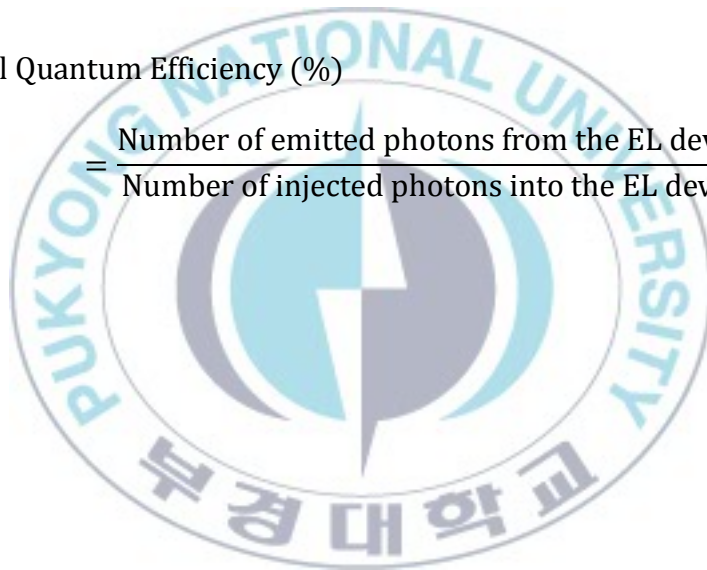
Figure 1-5. Parameters of PSC in J-V curve.

I-2-2. Parameters of Polymer Light-Emitting Diodes

When the electric field is applied to the PLED, significant current will flow at the certain voltage, which is defined as the turn-on voltage (V_{on}). The turn-on voltage and the external quantum efficiency of the devices depend on the energy difference between the work function of anode and the HOMO level and the energy difference between the work function of cathode and the LUMO level.

External Quantum Efficiency (%)

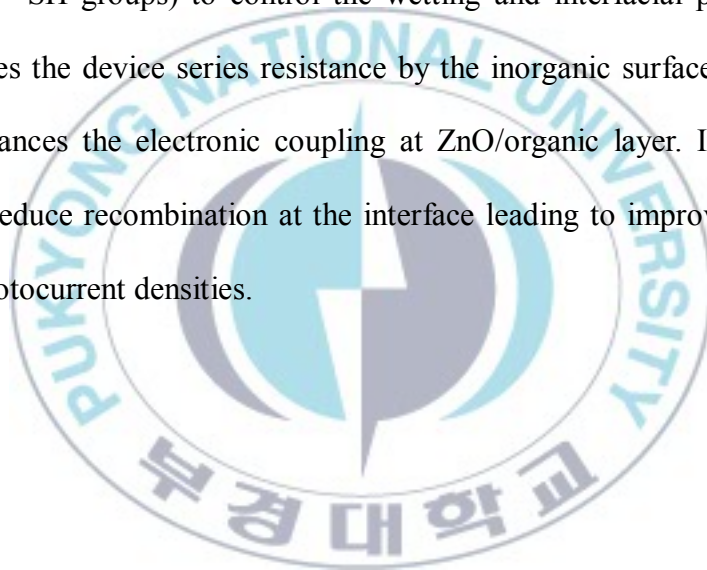
$$= \frac{\text{Number of emitted photons from the EL device}}{\text{Number of injected photons into the EL device}} \times 100$$



I-3. Self-Assembled Monolayers

Self-assembled monolayer (SAM) of organic molecules is formed spontaneously on surfaces of the substrate by chemical adsorption. Covalent bond appears the interfacial layer between the surface of substrate and the functional group of self-assembled molecule. Typically, SAM molecule are connected to a molecular chain in which the terminal end can be functionalized (i.e. $-\text{OH}$, $-\text{NH}_2$, $-\text{COOH}$, or $-\text{SH}$ groups) to control the wetting and interfacial properties. The SAM reduces the device series resistance by the inorganic surface trap states as well as enhances the electronic coupling at ZnO/organic layer. It helps charge transfer to reduce recombination at the interface leading to improved fill factors (FF) and photocurrent densities.

[



I-4. Measurement

Synthesized compounds were characterized by ^1H NMR and ^{13}C NMR spectra, which were obtained with a JEOL JNM ECP-400 spectrometer. The thickness of the film was measured by an Alpha-Step IQ surface profiler (KLA-Tencor Co.). Elemental analysis of before and after SAM treatment by the benzoic acid derivatives was performed using (THERMO VG SCIENTIFIC (UK), MultiLab2000) X-ray photoelectron spectroscopy (XPS) and recorded using Al $K\alpha$ X-ray line (15 kV, 300 W). The work function measurements were carried out using a UPS (VG Scientific Co.) with a He I source ($h\nu = 21.2$ eV) at a pressure of 1×10^{-8} Torr. A -3 V was applied to a sample during the measurements to distinguish between the analyzer and sample cut-off. The surface energy (γ) of the ZnO layer before and after SAM treatment was evaluated by the measurements of the static advancing contact angle with deionized water and diiodomethane. The contact angles (KRUSS, Model DSA 100) were entered in the Wu model (harmonic mean) for the calculation of the dispersive and polar components of the surface energy. The effective work function was obtained by Kelvin probe (KP) measurements (McAllister Technical Services, KP 6500) of the contact potential difference between the sample and the KP tip. The KP tip work function was 5.203 ± 0.011 eV. TEM images of the P3HT:PCBM active layer were obtained with a JEM-2010 using an accelerating

voltage of 80 kV. The active layer was delaminated from the ITO substrate by dissolving the ZnO layer in HCl solution. The typical thickness of delaminated films for TEM was ca. 200 nm. The AFM topography images were taken using a Digital Instruments (Multi Mode SPM) operated in the tapping mode. The current density–voltage measurements under 1.0 sun (100 mW/cm²) condition from a 150 W Xe lamp with a 1.5 G filter were performed using a KEITHLEY model 2400 source measure unit. A calibrated Si reference cell with a KG5 filter certified by the National Institute of Advanced Industrial Science and Technology was used to confirm 1.0 sun condition. The incident photon to collected electron efficiency (IPCE), external quantum efficiency, was calculated by

$$\text{IPCE (\%)} = 1240 \times J_{sc} / \left(\frac{\lambda}{I_p} \right)$$

where J_{sc} ($\mu\text{A}/\text{cm}^2$) is the short circuit current density measured at the wavelength λ (nm) and I_p (W/m^2).

Chapter II. Inverted type Polymer Solar Cells Using Self-Assembled Monolayer treated ZnO with Benzoyl Chloride Derivatives as Electron Transporting Materials

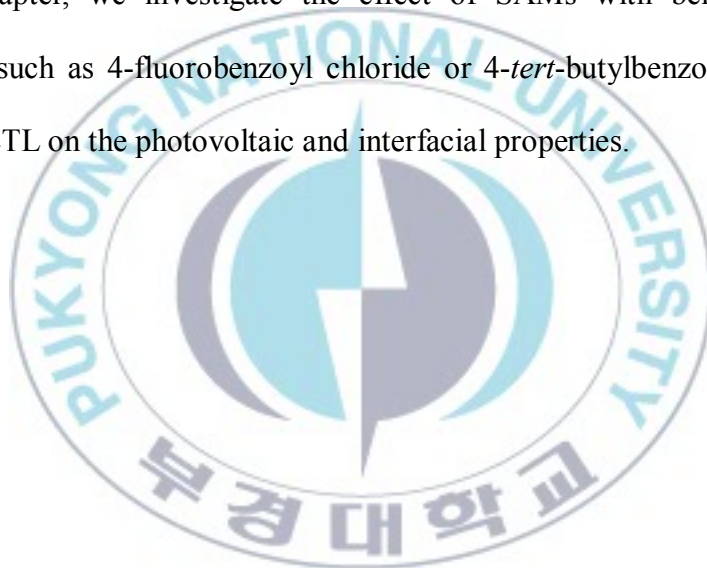
II-1. Introduction

Recently, polymer solar cells (PSC) are attractive as an energy source, because it has many advantages, containing low fabrication cost and application in flexible devices.¹⁻⁸ Bulk hetero junction (BHJ) PSC comprising conjugated polymer as an electron donor such as poly(3-hexylthiophene-2,5-diyl) (P3HT) and fullerene derivative as an electron acceptor such as [6,6]-phenyl-C61-butyric acid methyl ester (PCBM).⁹⁻¹² In BHJ structure, a thin layer of LiF¹³⁻¹⁵, poly(ethyleneoxide)¹⁶, water soluble π -conjugated polymers¹⁷⁻¹⁹ and water soluble non-conjugated polyelectrolyte based on viologen^{20,21} as for the cathode. These days many research have been reported to improve performance of the devices by development of new materials²²⁻²⁶, using low work function metal and optimization of interface^{27,28}. Usually, CPSCs are required low work function metal as a top cathode to efficient electron extraction. Because these electrode metals are poor stability and hole transporting materials such as poly(3,4-ethylenedioxythiophene):poly(styrenesulfonate) (PEDOT:PSS)²⁹ are poor stability which is acidic material, this structure is not suitable for large area processing. To resolve this problem, inverted-PSC using metal oxide as electron

transporting layer (ETL) with opposite current flow are used many research.³⁰⁻³²

A buffer layer is used to optimize interface between active layer and electrodes to expedite charge collect and extraction such as TiO_x and ZnO instead of PEDOT:PSS.³³ To control morphology in PSC, many research introduce many skill such as using nanoparticle,^{34,35} additives^{36,37}, co-solvent and self-assembles monolayer (SAM)³⁸⁻⁴³.

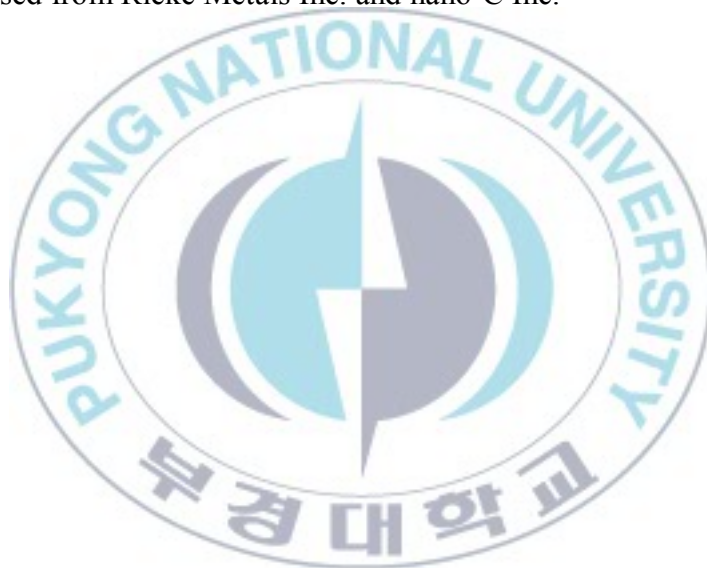
In this chapter, we investigate the effect of SAMs with benzoyl chloride derivatives such as 4-fluorobenzoyl chloride or 4-*tert*-butylbenzoyl chloride on ZnO as an ETL on the photovoltaic and interfacial properties.



II-2. Experiment Section

II-2-1. Materials

4-*tert*-Butylbenzoyl chloride, 98% was purchase from Sigma Aldrich. 4-Fluorobenzoyl chloride, 98%, zinc acetate dihydrate, triethanol amine, and methoxyethanol were purchased from Alfa Aesar Regioregular poly(3-hexylthiophene) (P3HT) and (6,6)phenyl-C₆₁-butyric acid methyl ester (PC₆₁BM) were purchased from Rieke Metals Inc. and nano-C Inc.



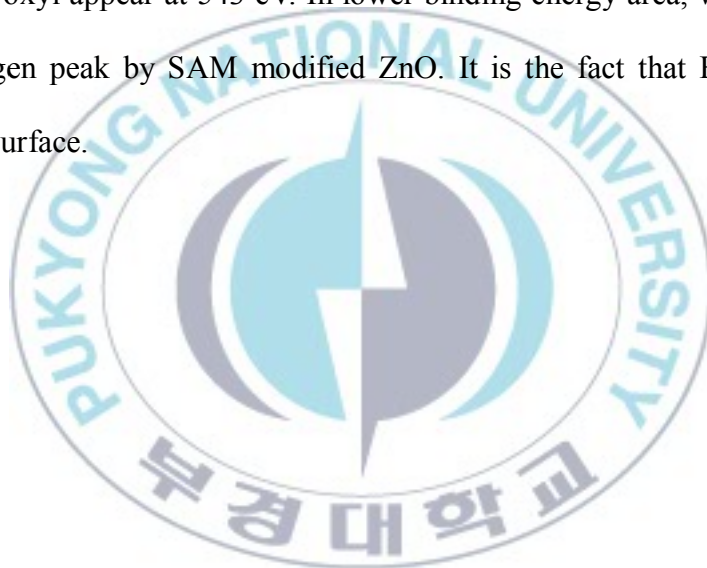
II-2-2. Fabrication of IPSCs

To fabricate inverted polymer solar cells, we prepared indium tin oxide (ITO)/glass (sheet resistant = 15 ohm/square) as electrode substrate which was cleaned in deionized water, methanol, acetone and isopropanol successively by sonicator for 10 minutes. A Zinc oxide (ZnO) was synthesized with 0.164 g of zinc acetate dihydrate and 0.05 mL of ethanolamine dissolved in 1.0 mL of methoxyethanol by simple sol-gel process. And then the ZnO solution was stirred at 60 °C for 30 min in an air atmosphere. A ZnO layer of 40 nm was spin-coated on ITO pre-treated UV/O₃ and cured 300 °C for 10 min to crystallize the ZnO film by literature process.^{33, 42} The electron transporting layer was changed by using self-assembled molecules such as 20 μL of 4-fluoro-benzoyl chloride (FBC) and 4-*tert*-Butyl-benzoylchloride (BBC) in 1 mL of toluene by dipping. To remove remains SAM solution, we rinsed with methanol and dried air. The ratio of P3HT and PC₆₁BM layer on ZnO/SAM layer was 1:1 with concentration of 20 mg/mL in 1,2-dichlorobenzene at 600 rpm for 40 s and dried in room temperature for 1 hour. Before thermal evaporation of WO₃ and Ag, the film was annealed at 160 °C for 10 min in glovebox. On the active layer, WO₃ of 20 nm and Ag of 100 nm were deposited with effective area 0.12cm² at 2 × 10⁻⁶ Torr.

II-3. Results and Discussion

II-3-1. Characterization of SAM modified ZnO

To confirm covering SAMs on ZnO surface, we measure X-ray photoelectron spectroscopy (XPS). Figure 2-1 shows the oxygen peaks in XPS are asymmetric, because there are two oxygen species in the ZnO surface. The oxygen peak in the ZnO crystal lattice appear at 540 eV and the chemisorbed oxygen peak caused by surface hydroxyl appear at 543 eV. In lower binding energy area, we confirm the shifted oxygen peak by SAM modified ZnO. It is the fact that BBC and FBC cover ZnO surface.



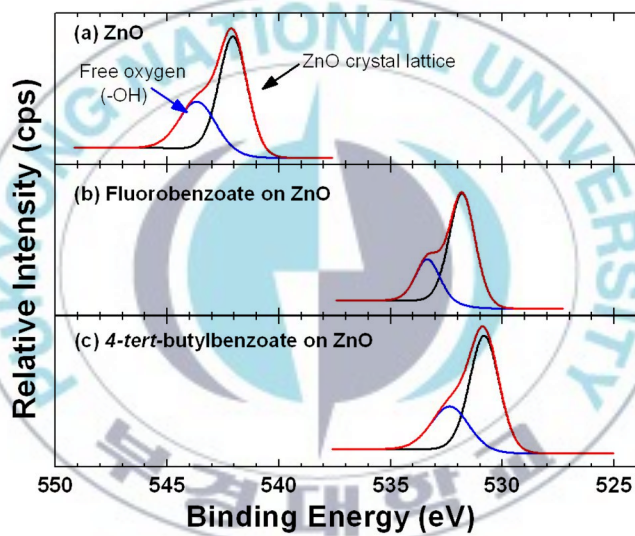


Figure 2-1. O_{1s} XPS spectra of (a) ZnO, (b) FBC treated ZnO and (c) BBC treated ZnO.

The important factor for improving the device performances is the reduction of the electron injecting barrier. An interfacial dipole moment between ZnO and the active layer can be modified by SAM with different dipole direction. In Figure 2-2, ZnO/FBC/active layer with an interfacial dipole moment shifted away from the active layer. On the contrary, ZnO modified BBC has exactly opposite direction of interfacial dipole moment with that of FBC case. We measured ultraviolet photoelectron spectroscopy (UPS) to confirm the work function of ZnO and SAM coated ZnO surface to confirm the interfacial dipoles. Figure 2-3 shows the work function calculated by cut-off energy and Fermi level in UPS spectra. The work function of ZnO treated FBC is larger than that of ZnO. In contrary, the work function of BBC coated ZnO is smaller than that of ZnO without SAM. By covering benzoyl chloride derivates, the surface potential of inorganic semiconductor can be changed.

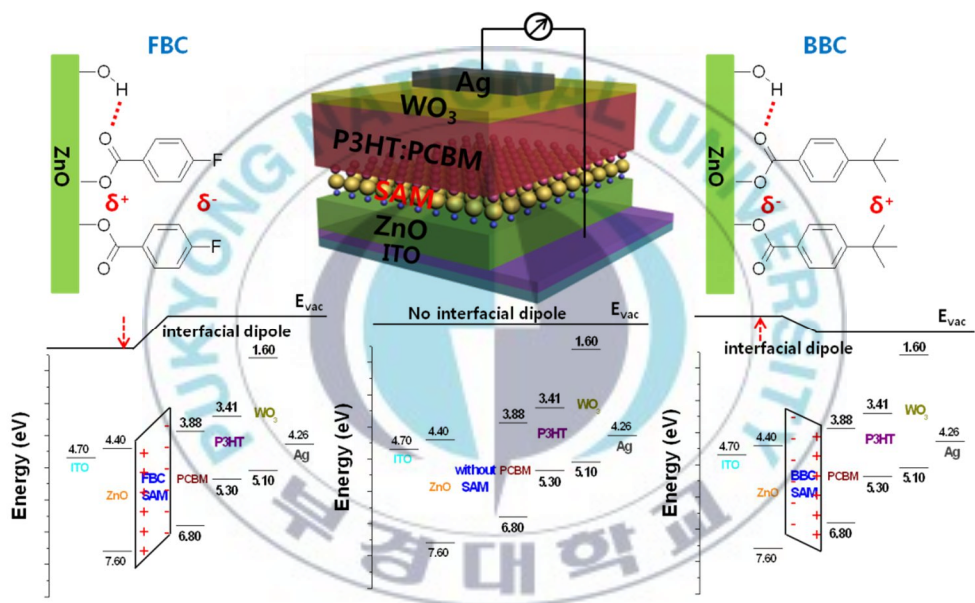


Figure 2-2. The devices structures and the chemical structures used in the device fabrications and energy diagram of ITO/ZnO/P3HT:PCBM/WO₃/Ag device with or without SAM.

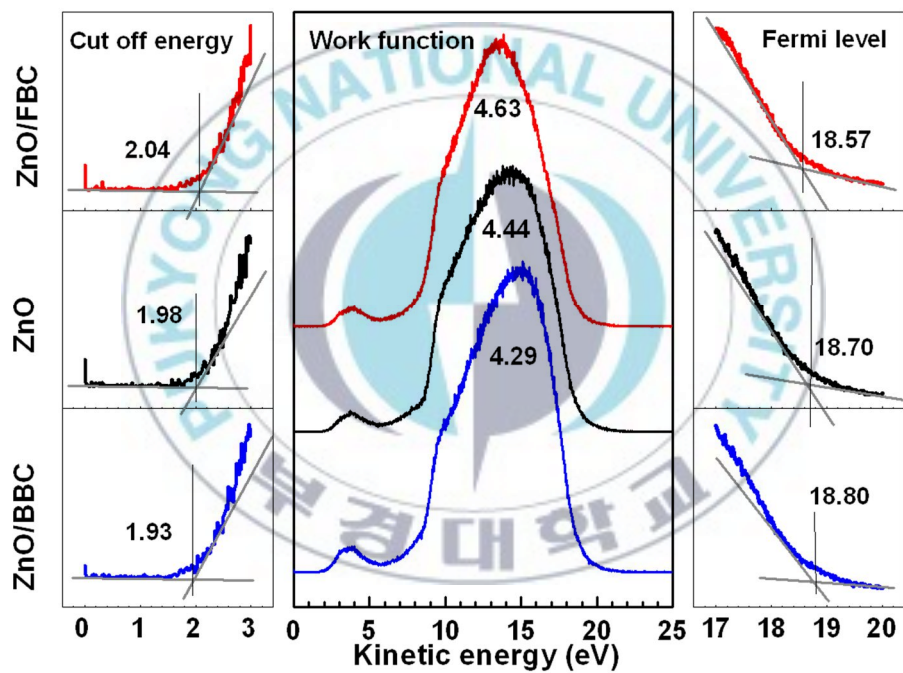


Figure 2-3. UPS spectra of ZnO, FBC coated ZnO and BBC coated ZnO.

II-3-2. Photovoltaic Properties of IPSCs

Figure 2-4 shows the current density-voltage curves of inverted solar cells with SAM treated ZnO. We summarize the best performance and average data in Table 2-1. As shown in Table 2-1, the V_{oc} of FBC treated ZnO (0.54 V) lower than that of no SAM (0.59 V) and BBC on ZnO (0.58 V). This is because FBC treated ZnO is not efficient by an unreliable formation of dipole direction. The power conversion efficiency (PCE) of inverted solar cells with BBC on ZnO as an ETL is higher than that of devices without SAM and with FBC on ZnO. The best PCE presenting Table 2-1 reaches 2.99% increasing 19.12% compared with the device with bare ZnO. On the other hand, the performance of the device using FBC is lower than that of the device with bare ZnO layer (Figure 2-4 and Table 2-1).

The series resistance (R_s) and parallel resistance are important parameter in PSCs. In the dark J-V curve, R_s and R_p were calculated from the inverse slope around high current area and the slope around low current area (Figure 2-4 (b)). The R_s value of the devices with ZnO, FBC on ZnO and BBC on ZnO are 4.18, 3.77 and 3.41 $\Omega \cdot \text{cm}^2$, respectively. In conclusion, the devices with ZnO/BBC shows best optimized performance of inverted PSC with ZnO as an ETL.

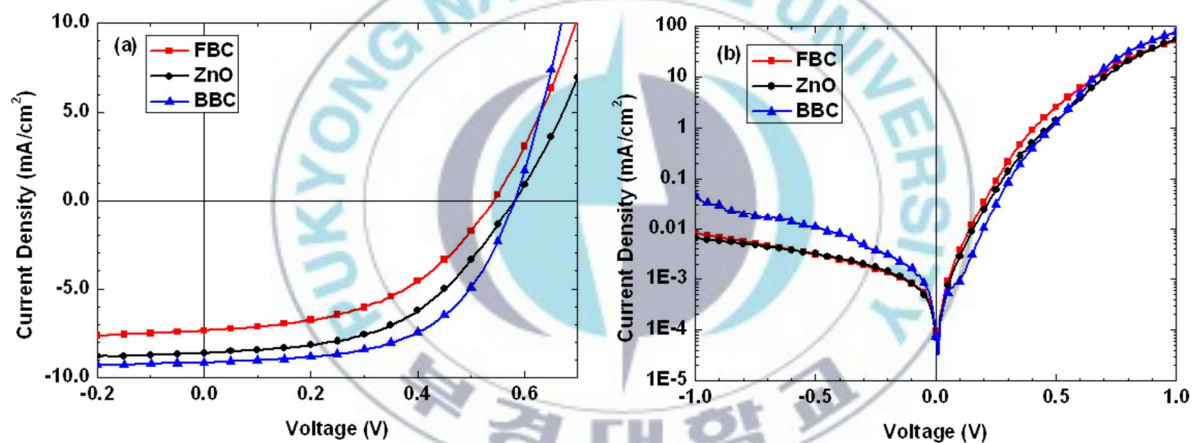


Figure 2-4. Current density–voltage curves of PSCs (a) under AM 1.5G simulated illumination with an intensity of 100mW/cm² and (b) under the dark condition (rectangle: without SAM treatment, circle: with FBC treated from solution of 20 μ l/ml and triangle: with BBC treated from solution of 20 μ l/ml)

Table 2-1. Photovoltaic properties of inverted solar cells treated FBC and BBC.

	V_{oc} (V)	J_{sc} (mA/cm ²)	FF (%)	PCE (%)	R_s ($\Omega \cdot \text{cm}^2$) ^a	R_p (k $\Omega \cdot \text{cm}^2$) ^b	n^c	J_s (mA/cm ²) ^d
FBC	0.54 (0.52±0.013)	-7.367 (-7.152±0.129)	47.8 (47.1±0.813)	1.90 (1.76±0.078)	3.77	420.17	1.82	0.019
ZnO	0.58 (0.59±0.005)	-8.629 (-7.726±0.396)	50.2 (54.3±2.054)	2.51 (2.43±0.068)	4.18	164.47	2.97	2.018
BBC	0.58 (0.58±0.000)	-9.141 (-9.025±0.082)	56.5 (55.3±0.800)	2.99 (2.89±0.055)	3.41	36.19	2.39	0.435

^a: series resistnace (estimated from the devices with best PCE value).

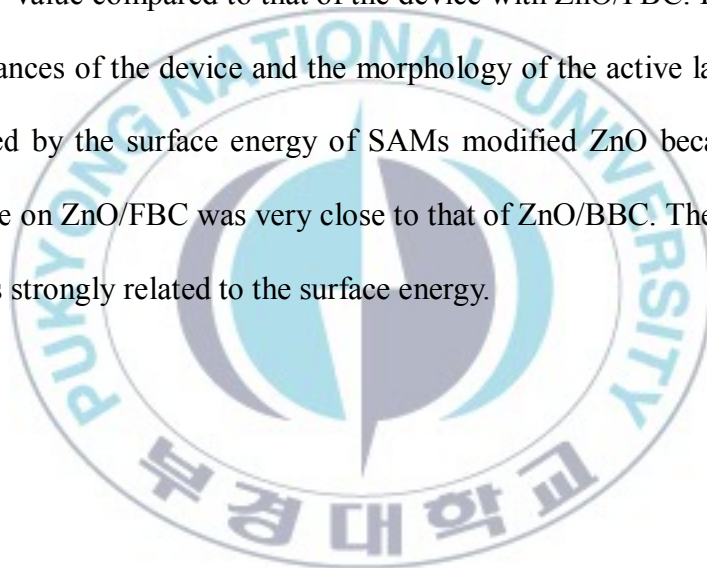
^b: paralell resistance (estimated from the devices with best PCE value).

^c: ideality factor.

^d: saturation current density

II-3-3. Surface Properties of the Active Layer

Figure 2-5 shows contact angle of ZnO surface without SAM treatment and with two types of SAM treatment. The static water contact angle of ZnO, FBC coated ZnO and BCC coated ZnO is ($33.95^\circ \pm 1.18^\circ$), ($68.67^\circ \pm 0.56^\circ$) and ($55.46^\circ \pm 0.52^\circ$). By using SAM treatment, the ZnO surface is more hydrophobic than the ZnO untreated SAM. Thus, the device with bare ZnO and ZnO/BBC showed better the FF value compared to that of the device with ZnO/FBC. In this research, the performances of the device and the morphology of the active layer seemed to be unaffected by the surface energy of SAMs modified ZnO because the water contact angle on ZnO/FBC was very close to that of ZnO/BBC. The water contact angle data is strongly related to the surface energy.



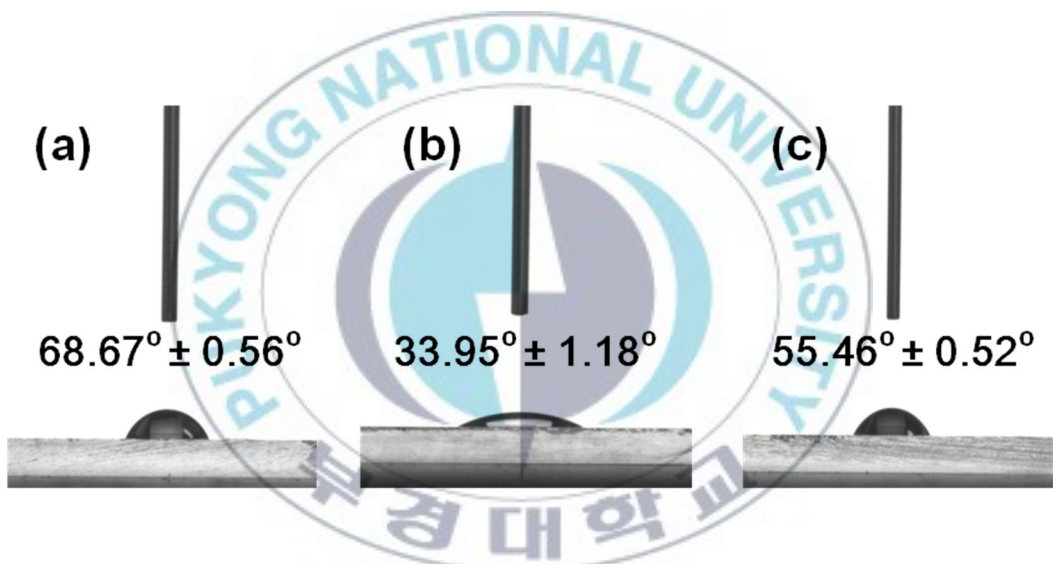
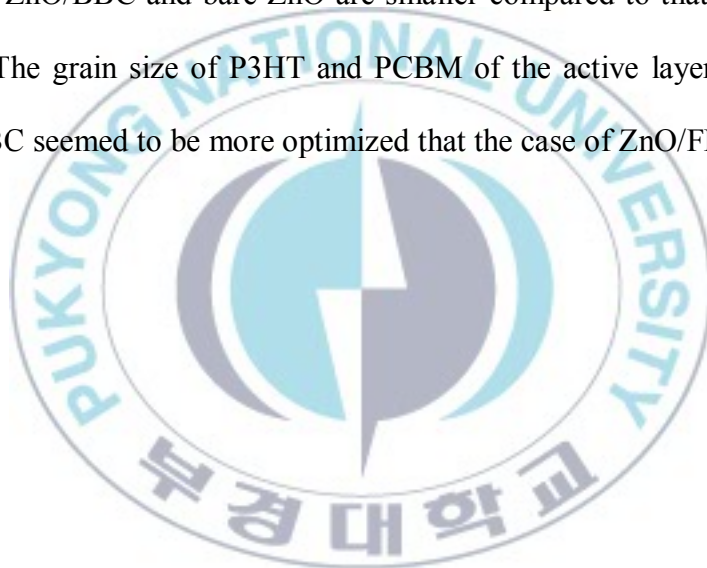


Figure 2-5. Contact angle of (a) FBC on ZnO surface, (b) ZnO surface and (c) BBC on ZnO surface (water drop on the top of ZnO, FBC and BBC)

Atomic force microscopy (AFM) images were taken to investigate the morphology of the active layer on SAMs treated ZnO. The root-mean-square (RMS) roughness of the active layer on ZnO/FBC was 9.50 nm, which was much higher than that of the active layer on bare ZnO (4.93 nm) and ZnO/BBC (5.33 nm). The surface morphology reflects the grain size of P3HT and PC₆₁BM. From the RMS roughness data and the surface morphology, the grain size of P3HT and PC₆₁BM on ZnO/BBC and bare ZnO are smaller compared to that of the case of ZnO/FBC. The grain size of P3HT and PCBM of the active layer on bare ZnO and ZnO/FBC seemed to be more optimized than the case of ZnO/BBC.



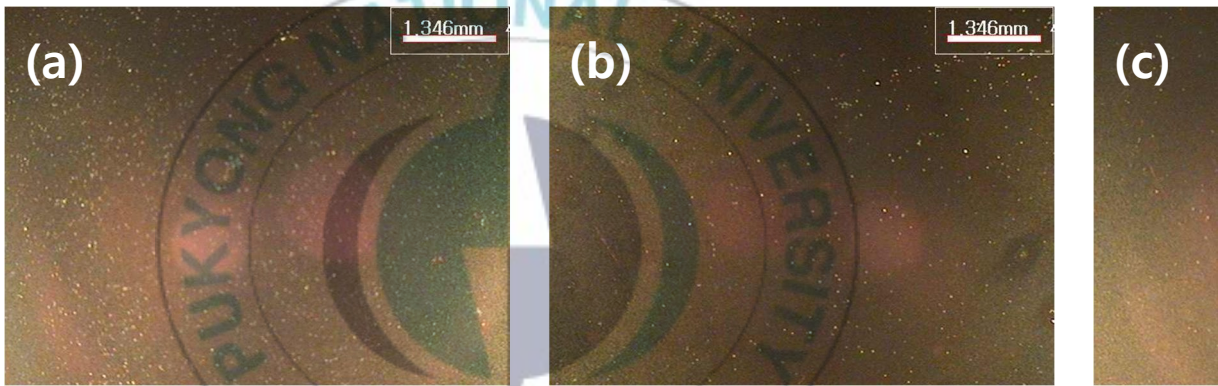


Figure 2-6. Optical microscope images of ITO/ZnO(FBC orBBC)/P3HT:PCBM surface. (X40)

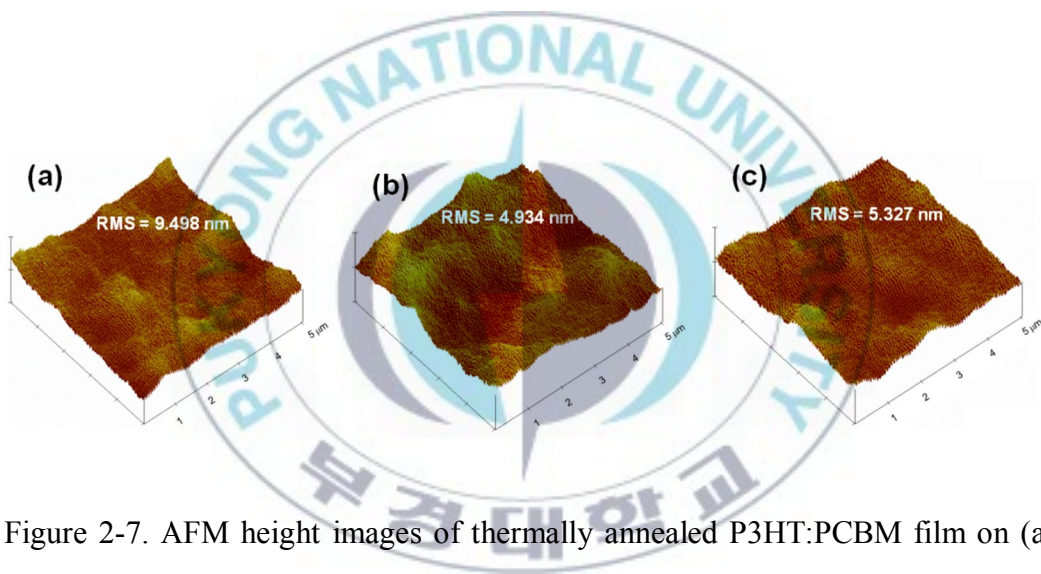
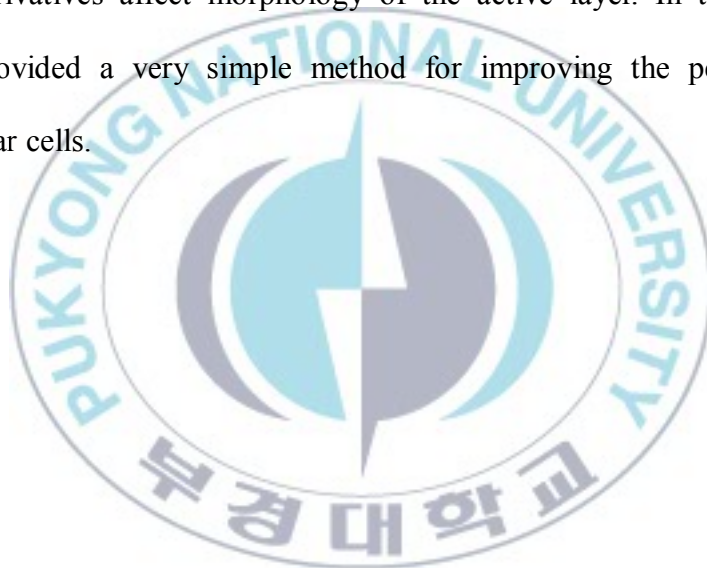


Figure 2-7. AFM height images of thermally annealed P3HT:PCBM film on (a) ZnO/FBC (b) ZnO and (c) ZnO/BBC.

II-4. Conclusion

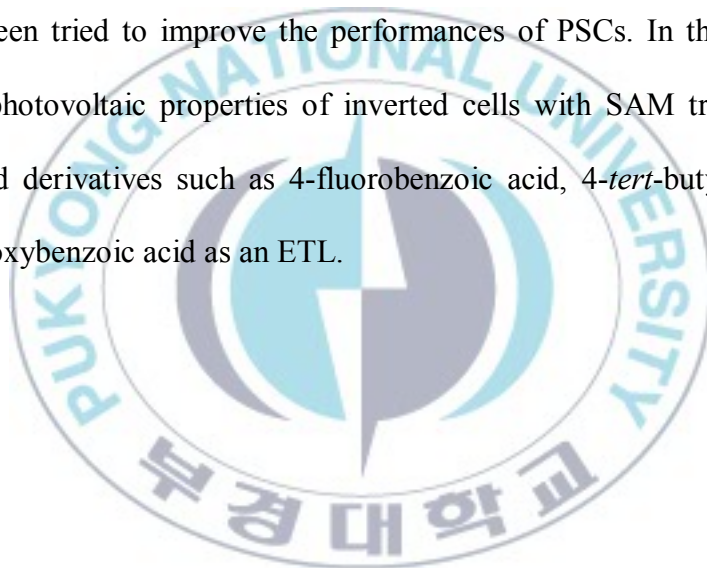
We have investigated inverted polymer solar cells with benzoyl chloride derivatives SAM treated ZnO as an electron transporting layer. By the interfacial dipole orientation, the work function and morphology of ZnO can be changed. The work function of ZnO depends on dipole direction in the interface between ZnO and P3HT:PC₆₁BM layer. In addition, we have checked that benzoyl chloride derivatives affect morphology of the active layer. In this paper, our research provided a very simple method for improving the performance of inverted solar cells.



Chapter III. Inverted type Polymer Solar Cells Using Self-Assembled Monolayer treated ZnO with Benzoic Acid derivatives as Electron Transporting Materials

III-1. Introduction

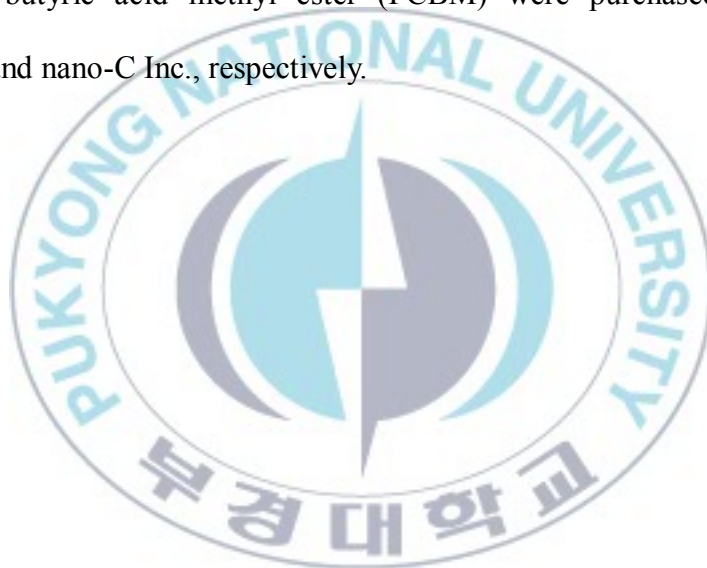
Nanoparticle,^{44,45} additives^{46,47}, co-solvent and self-assembled monolayer (SAM)⁴⁸⁻⁵³ have been tried to improve the performances of PSCs. In this chapter, we report the photovoltaic properties of inverted cells with SAM treated ZnO by benzoic acid derivatives such as 4-fluorobenzoic acid, 4-*tert*-butylbenzoic acid and 4-methoxybenzoic acid as an ETL.



III-2. Experiment Section

III-2-1. Materials

4-Fluorobenzoic acid (FBA), 4-*tert*-butylbenzoic acid (BBA), 4-methoxybenzoic acid (MBA), zinc acetate dihydrate, triethanol amine, and methoxyethanol were purchased from Alfa Aesar and used as received unless otherwise described. Regioregular poly(3-hexylthiophene) (P3HT) and (6,6)-phenyl-C61-butyric acid methyl ester (PCBM) were purchased from Rieke Metals Inc. and nano-C Inc., respectively.



III-2-2. Fabrication of IPSCs

For fabrication of PSCs with a structure of ITO/before and after SAM treated ZnO/active layer/MoO₃/Ag, a layer of 40 nm thick ZnO film on precleaned and UV/O₃ treated ITO (sheet resistance = 13 ohm/square) was deposited by using the sol-gel process. The sol-gel solution was prepared with 0.164 g of zinc acetate dehydrate and 0.05 mL of ethanolamine dissolved in 1 mL of methoxyethanol. The solution was stirred for 30 min at 60 °C prior to deposition. The thin film of ZnO precursor was cured at 300 °C for 10 min to partly crystallize the ZnO film, which is prepared by the literature procedures.^{43,32} To deposit self-assembled molecules, a 1.0 mg/mL solution of benzoic acid derivative in methanol was spin-coated on the ZnO film at 4000 rpm for 60 s. To remove physically absorbed molecules, the SAM treated ZnO surface was washed using pure methanol and then dried by the stream of nitrogen. The active layer was spin cast from the blend solution of P3HT/PCBM (20 mg of P3HT and 20 mg of PCBM were dissolved in 1 mL of o-dichlorobenzene (ODCB)) at 600 rpm for 40 s and dried in a covered Petri dish for 1 h. Prior to spin coating, the active solution was filtered through a 0.45 μm membrane filter. The typical thickness of the active layer was 200 nm. Before deposition of MoO₃/Ag, the active layer was thermally annealed at 150 °C for 20 min in the glovebox (N₂ atmosphere). Finally, 20 nm thick MoO₃

and 100 nm thick Ag were deposited successively onto the top of the active layer through a shadow mask with a device area of 0.13 cm^2 at 2×10^{-6} Torr.



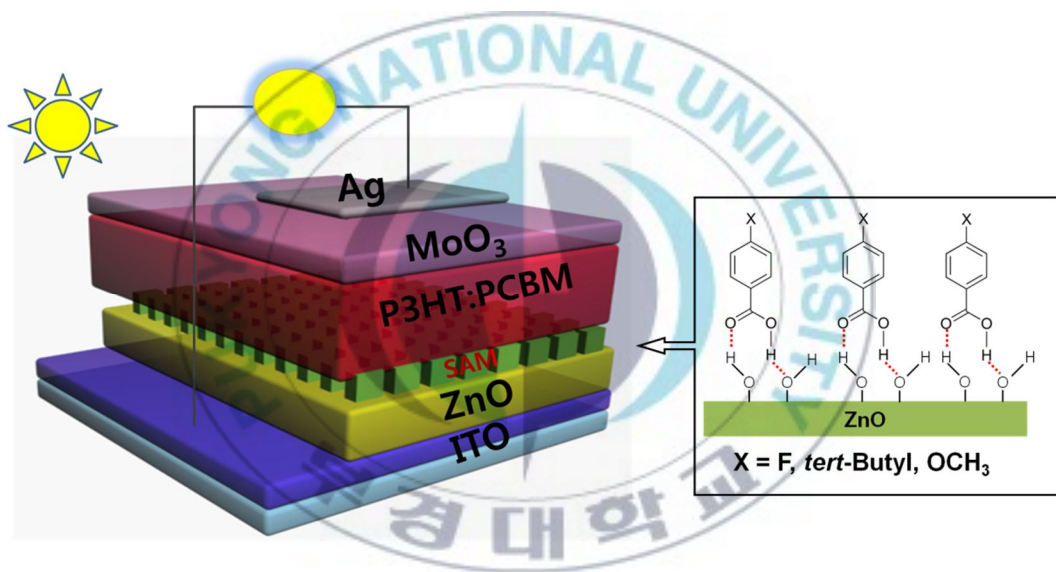


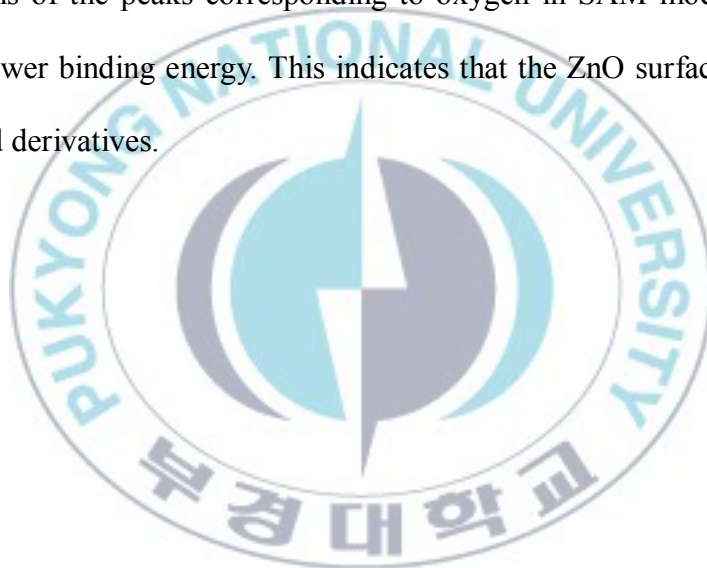
Figure 3-1. Structure of Devices and Self-Assembled Molecules

III-3. Results and Discussion

III-3-1. Characterization of SAM modified ZnO

As shown in Figure 3-2, XPS spectra were measured to confirm coating by the SAM of the ZnO surface. The oxygen peaks that there are two oxygen species in ZnO are asymmetric. The peaks at 542 eV is oxygen in the ZnO lattice, and the peak at 543 eV corresponds to adsorbed oxygen caused by surface hydroxyl.⁵⁴

The positions of the peaks corresponding to oxygen in SAM modified ZnO are shifted to lower binding energy. This indicates that the ZnO surface is coated by benzoic acid derivatives.



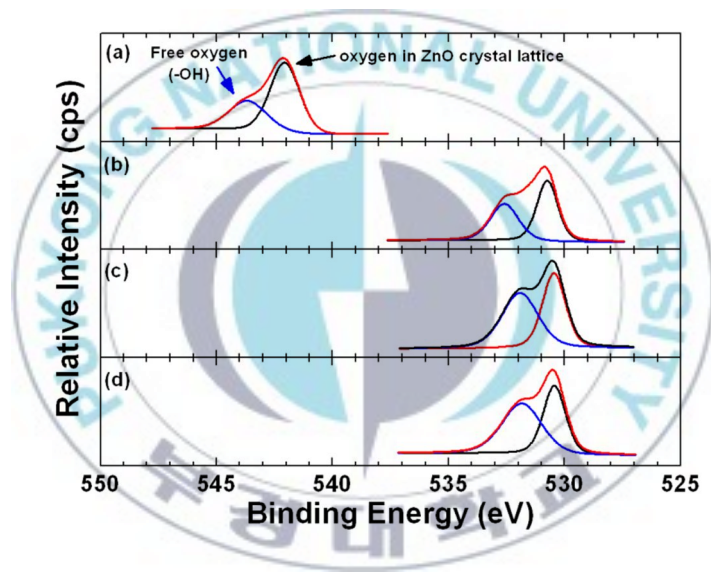


Figure 3-2. XPS spectra of (a) ZnO, (b) ZnO/FBA, (c) ZnO/BBA and (d) ZnO/MBA

One of the important things for improving the device performances is the charge barrier in PSC. In Figure 3-3, the electron injection barrier can be control by the formation of dipole moment between ZnO and active layer. We measured the effective work function of ZnO and SAM modified ZnO surface by using Kelvin Probe Microscope (KPM) in order to confirm the formation of interfacial dipole by SAM treatment. As shown Figure 3-4, the effective work function ZnO treated FBA is 4.31 ± 0.04 eV, which is larger than that of ZnO (4.17 ± 0.01 eV). The effective work functions of ZnO treated BBA and MBA are 3.97 ± 0.01 and 3.94 ± 0.04 eV, which are smaller than that of untreated ZnO. The interfacial dipole orientation of FBA and BBA (or MBA) is the opposite direction. In case of FBA, the interfacial dipole moment between ZnO and the active layer is directed toward ZnO surface. On the contrary, the effective work functions of BBA and MBA treated ZnO is directed toward the active layer. We confirm that the dipole moment of benzoic acid derivatives reflects the electron-withdrawing and – donating power of the substituent. The strong electron-donating power substituent on benzoic acid reduces the surface potential and work function.

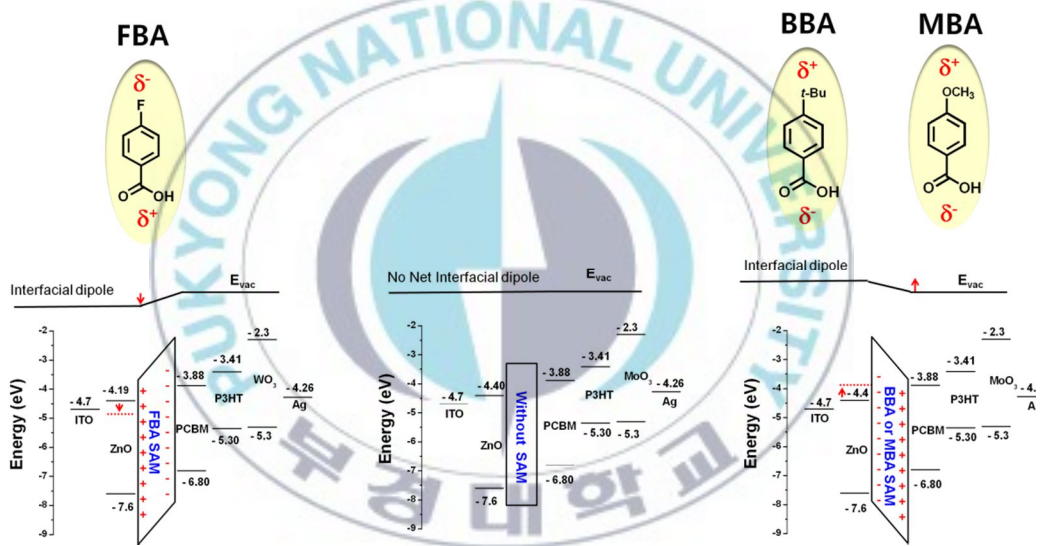


Figure 3-3. Interfacial dipole direction between ZnO and the active layer.

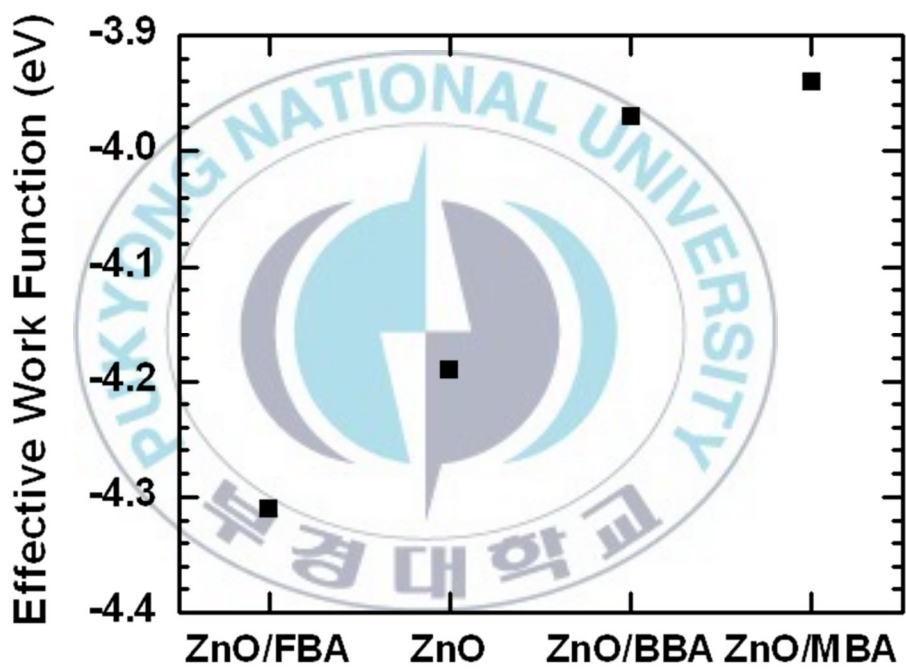


Figure 3-4. Effective work function of ZnO/FBA, ZnO, ZnO/BBA and ZnO/MBA.

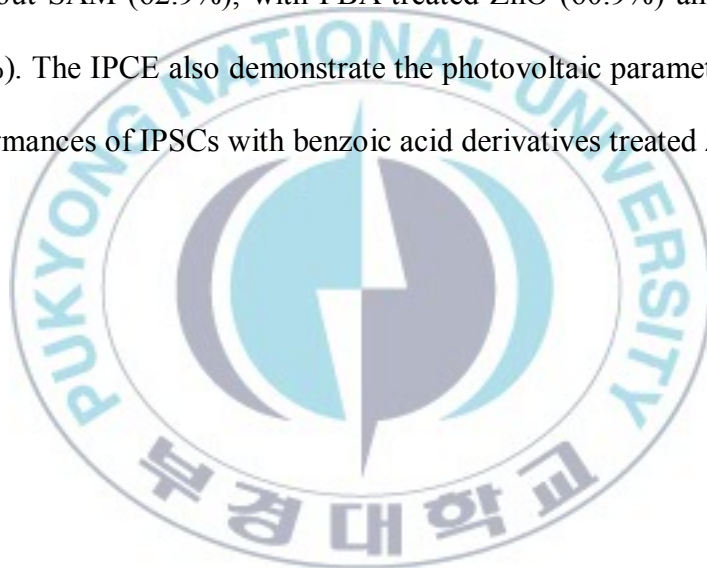
III-3-2. Photovoltaic Properties of IPSCs

Figure 3-5 shows current density – voltage curves of IPSCs under AM 1.5G simulated illumination with an intensity of 100 mW/cm^2 and under the dark condition. In Table 3-1 and Figure 3-6, the photovoltaic properties with SAM treated ZnO are summarized. The Power conversion efficiency (PCE) of IPSC with ZnO/MBA reaches 3.34%, which is higher than that of the device based on ZnO/FBA (1.81%), ZnO (2.49%), ZnO/BBA (2.94%). As shown in Table 1 and Figure 3-6 (a), the V_{oc} of the IPSC based on ZnO/MBA are 0.63 V, which is higher than those of IPSC with ZnO/BBA (0.62 V), ZnO (0.61 V) and ZnO/FBA (0.53 V). This is because the effective work function of ZnO/MBA shows the smallest value than the others. In case of ZnO/FBA, the V_{oc} is smaller than that of the devices untreated ZnO. This is due to the formation of an unreasonable interfacial dipole between ZnO and the active layer.

Short circuit current (J_{sc}) data of the devices are -7.55 mA/cm^2 (ZnO/FBA), -7.58 mA/cm^2 (ZnO), -7.88 mA/cm^2 (ZnO/BBA) and -8.77 mA/cm^2 (ZnO/MBA), respectively. The device with ZnO/MBA and ZnO/BBA shows better J_{sc} than that of the device based on ZnO. In contrary, the J_{sc} of the device with ZnO/FBA are very lower than that of the device with untreated ZnO. The fill factor data of the device with ZnO/FBA are 45.1%, which is also lower than that of the device untreated ZnO (51.5%). The FF of IPSCs with ZnO/BBA (60.4%) and ZnO/MBA (60.5%) are higher than that of the device based on ZnO. In case of ZnO/FBA,

the n and J_0 show the highest values. n is relation of the morphology between the polymers and the fullerenes. The saturation current density (J_0) represents the number of charge that can overcome the barriers under reverse bias.

Figure 3-7 shows the maximum of incident photon to collected electron efficiency (IPCE) of the IPSC at 540 nm. Among the IPSC, the device with MBA treated ZnO shows the highest value (65.1%), which is higher than that of the device without SAM (62.9%), with FBA treated ZnO (60.9%) and BBA treated ZnO (64.7%). The IPCE also demonstrate the photovoltaic parameters are related to the performances of IPSCs with benzoic acid derivatives treated ZnO.



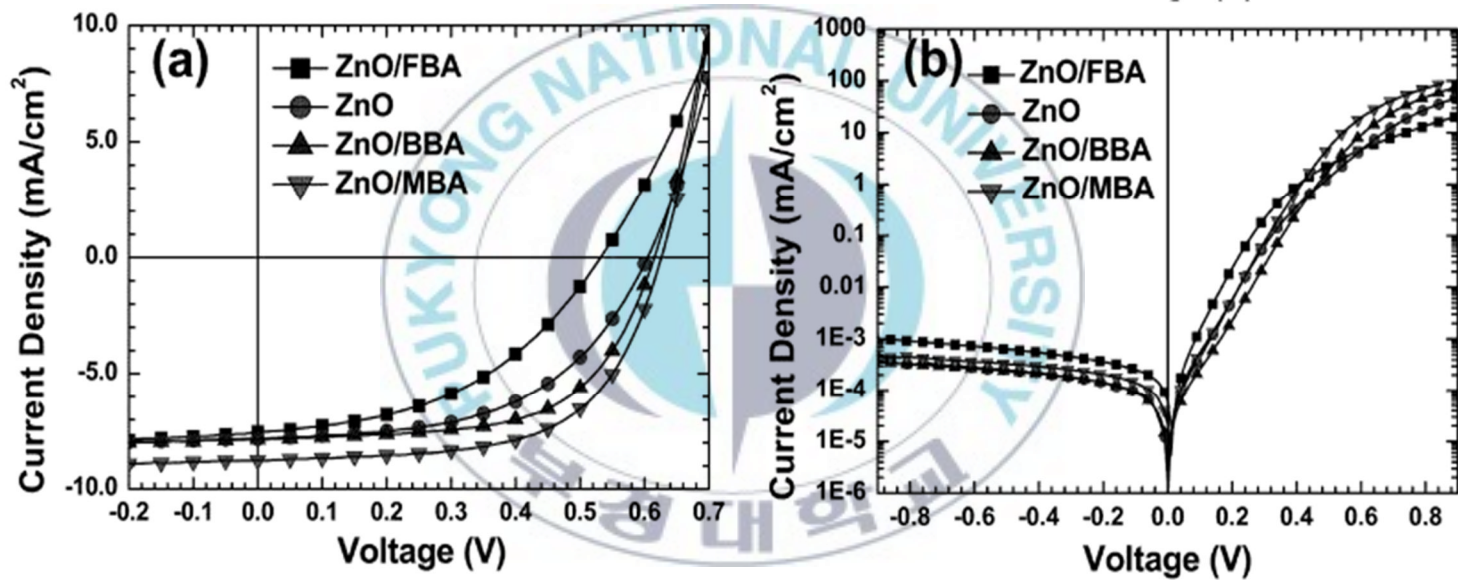


Figure 3-5. Current density-voltage curves of inverted type PSCs (a) under AM 1.5G simulated illumination with an intensity of 100 mW/cm² and (b) under the dark condition (square, FBA SAM modified; circle, without SAM; triangle, BBA SAM modified; inverted triangle, MBA SAM modified).

Table 3-1. The best photovoltaic parameters and efficiencies of PSC with various SAM treated ZnO. The averages for photovoltaic parameters of each device are given in parentheses with mean variation.

	V_{oc} (V)	J_{sc} (mA/cm ²)	FF (%)	PCE (%)	$R_s(\Omega \cdot \text{cm}^2)^a$	$R_p(\text{k}\Omega \cdot \text{cm}^2)^b$	n^c	J_s (mA/cm ²) ^d
FBA	0.53 (0.55 ± 0.01)	-7.55 (-7.23 ± 0.15)	45.1 (45.0 ± 0.43)	1.81 (1.78 ± 0.03)	13.7	1.03	2.37	0.93
No SAM	0.60 (0.61 ± 0.01)	-7.83 (-7.80 ± 0.07)	53.0 (51.6 ± 1.14)	2.49 (2.44 ± 0.07)	5.17	2.45	2.22	0.091
BBA	0.62 (0.62 ± 0.004)	-7.88 (-8.11 ± 0.17)	60.4 (57.6 ± 1.40)	2.94 (2.88 ± 0.05)	3.15	6.22	1.77	0.033
MBA	0.63 (0.62 ± 0.004)	-8.77 (-8.51 ± 0.13)	60.5 (59.8 ± 0.82)	3.34 (3.16 ± 0.06)	2.82	10.1	1.66	0.059

^a: series resistnace (estimated from the devices with best PCE value).

^b: paralell resistance (estimated from the devices with best PCE value).

^c: ideality factor.

^d: saturation current density

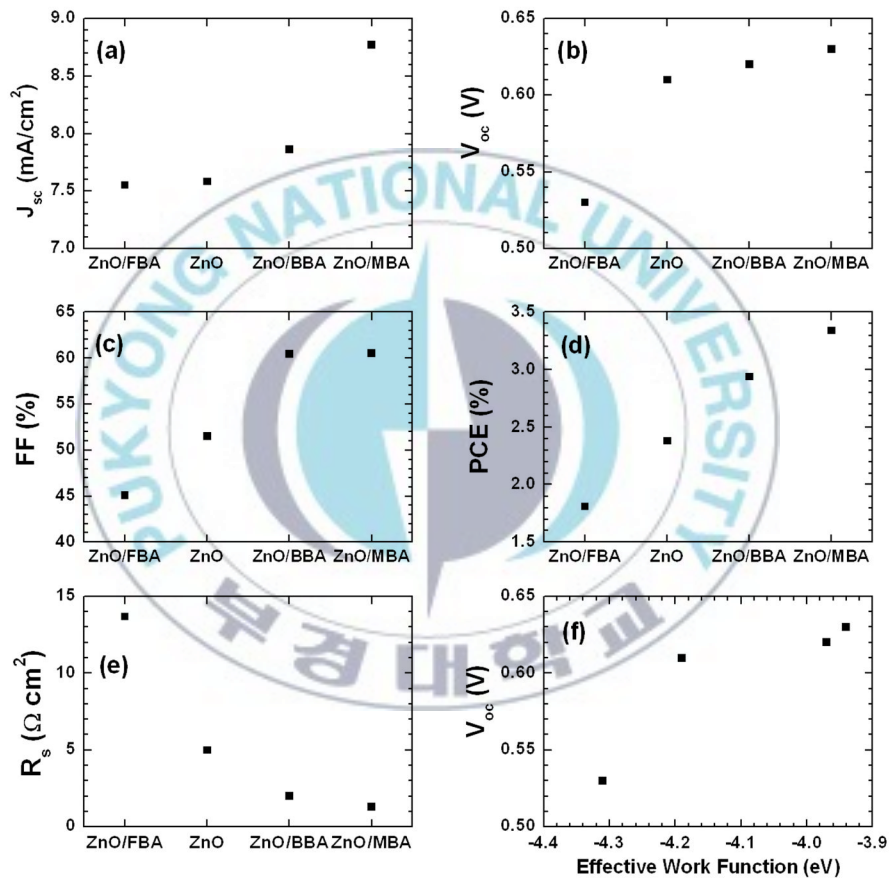


Figure 3-6. (a) J_{sc} , (b) V_{oc} , (c) FF, (d) PCE, (e) R_s and (f) V_{oc} vs. effective work function.

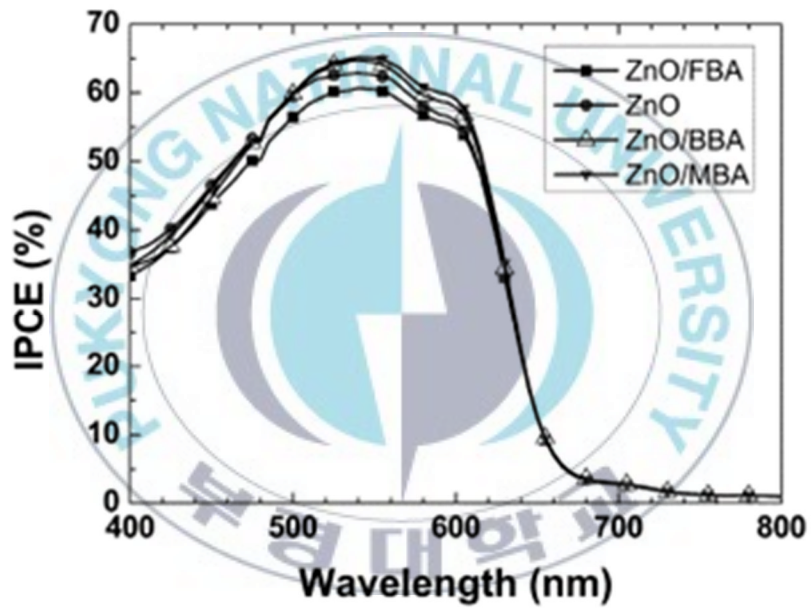


Figure 3-7. IPCE spectra of the devices ZnO/FBA, ZnO, ZnO/BBA and ZnO/MBA

III-3-3. Surface Properties of the Active Layer

For efficient charge transporting and separation in PSC, it should have phase separation of P3HT and PCBM in the order of 10 – 20 nm. To confirm the morphology of P3HT:PCBM, transmission electron microscope (TEM) and atomic force microscope (AFM) were measured by using the devices with BA SAM. Figure 3-8 shows TEM images of the phase separation of active layer. The active layer delaminated from the substrate by using HCl solution for remove a ZnO layer. In TEM images, the bright region indicates rich P3HT phase and the dark region indicates PCBM aggregation phase. A Figure 3-8 (a) has a very good interpenetrating network and phase separated active layer. However, the size of PCBM aggregation is 80 – 130 nm which is not reasonable phase distance. Figure 3-8 (c) and (d) show the active layer with BBA (30 - 40 nm) and MBA (10 – 20 nm), which is a reasonable distance for efficient charge separation of IPSC. Usually, the efficient active layer has thickness below 200 nm in PSC. In Figure 3-9 (a), the root means square (RMS) roughness of ZnO/FBA is 13.39 nm, which is supported that FF of the devices with FBA is lower than that of devices based on ZnO. In contrast, The RMS roughness of ZnO/BBA and ZnO MBA is 1.62 nm and 4.24 nm, which is not much different roughness of ZnO (2.89 nm). We confirm that ZnO/MBA exhibit optimized phase separated morphology among the devices by TEM and AFM images.

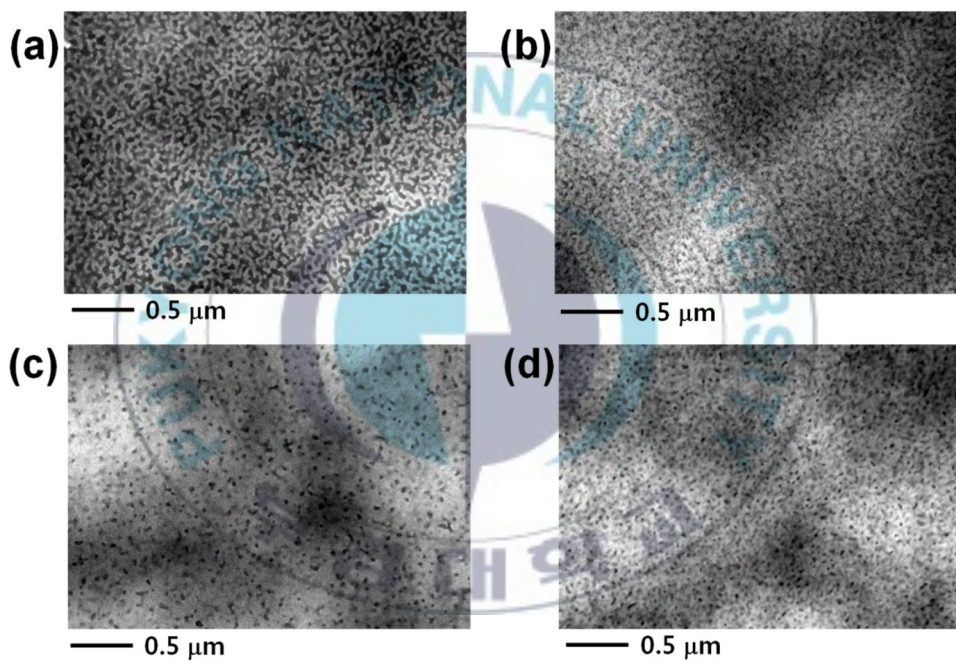


Figure 3-8. TEM images of the active layer deposited on (a) ZnO/FBA, (b) ZnO, (c) ZnO/BBA, and (d) ZnO/MBA.

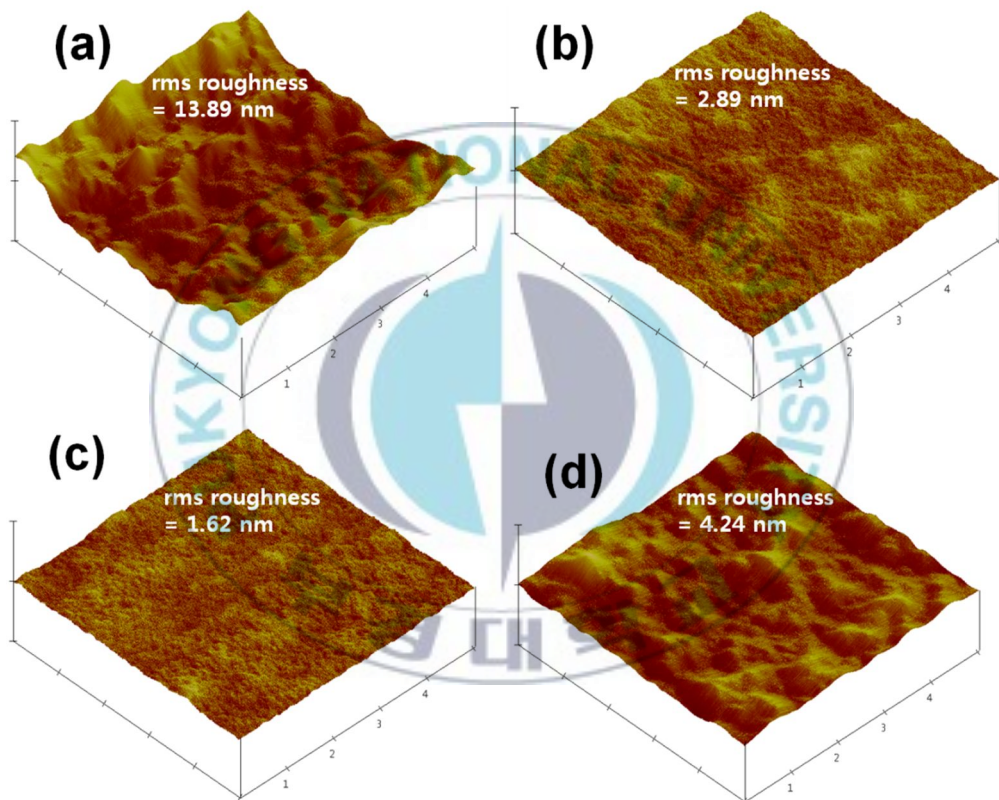


Figure 3-9. AFM topography images of thermally annealed P3HT/PCBM film on (a) ZnO/FBA, (b) ZnO, (c) ZnO/BBA, and (d) ZnO/MBA ($x, y = 1 \mu\text{m}/\text{div.}$, $z = 100 \text{ nm}/\text{div.}$).

As shown in Figure 3-10, the surface energy reflects the substituent on the benzoic acid derivatives. The surface energy of FBA treated ZnO (63.08 mN/m) is higher than that of untreated ZnO (45.37 mN/m). We expect that the active layer with FBA formation rough surface because ZnO/FBA has lower surface energy. In contrast, the surface energy of BBA (41.14 mN/m) and MBA (58.08 mN/m) is lower than that of devices with ZnO. BBA and MBA based on ZnO can help the stable formation of active layer due to higher surface energy.



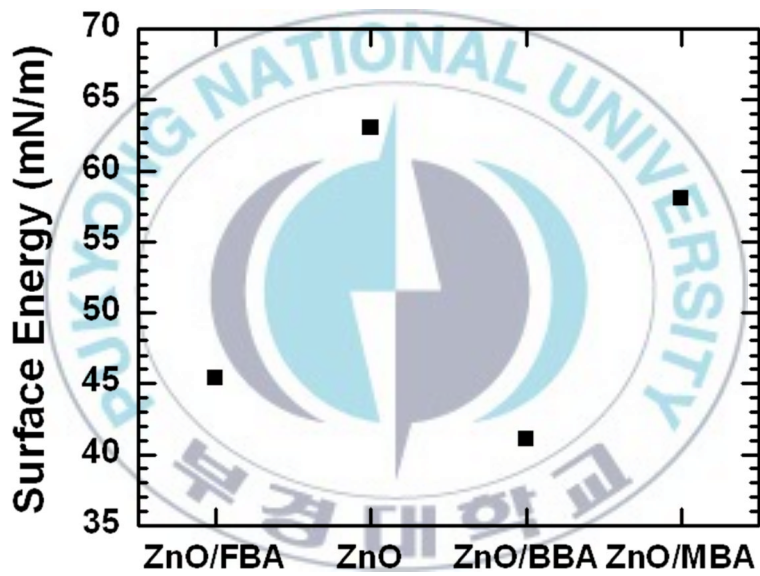


Figure 3-10. The surface energy of ZnO/FBA, ZnO, ZnO/BBA, and ZnO/MBA.

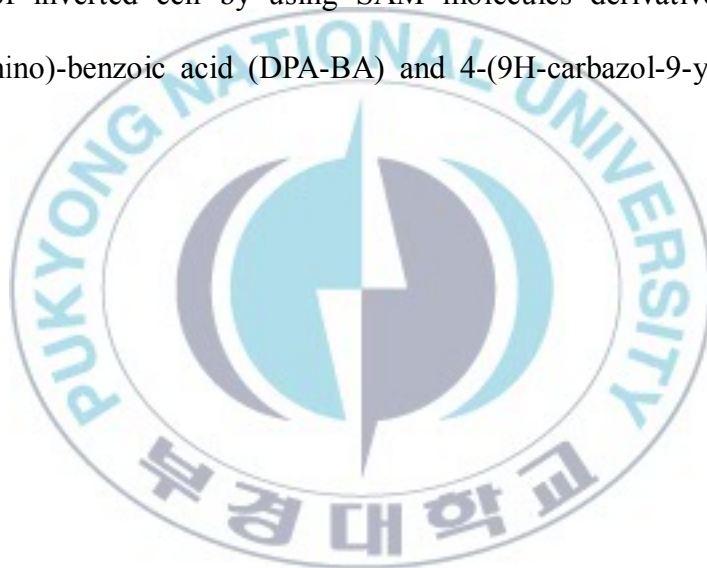
III-4. Conclusion

We have fabricated inverted polymer solar cells using by self-assembled monolayer with series of alkyl benzoic acid derivatives as an electron transporting layer. The effective work function and surface energy properties of ZnO can be successfully turned by the modification with SAM treatment of alkyl benzoic acid derivatives. The work function of ZnO depends on the orientation of the interfacial dipole between ZnO and the active layer. Also, we have demonstrated that the substituent on the 4-position of benzoic acid affects the morphology of the active layer. The performances of inverted polymer solar cells can be improved by the appropriate choice of self-assembled molecules. In this chapter, we provide an alternative strategy to improve the performances of inverted polymer solar cells by the control of interface property between inorganic and organic materials.

Chapter IV. Inverted type Polymer Solar Cells Using Self-Assembled Monolayer treated ZnO with Aryl Benzoic Acid Derivatives as Electron Transporting Materials

IV-1. Introduction

By using the same method in chapter II and III, we investigate the photovoltaic properties of inverted cell by using SAM molecules derivatives such as 4-(diphenylamino)-benzoic acid (DPA-BA) and 4-(9H-carbazol-9-yl)benzoic acid (Cz-BA).



IV-2. Experiment Section

IV-2-1. Materials

All other chemicals were purchased from Sigma-Aldrich Co, Tokyo Chemical Industry (TCI) or Alfa Aesar and used as received unless otherwise described. Regioregular poly(3-hexylthiophene) (P3HT) and (6,6)-phenyl-C61-butyric acid methyl ester (PCBM) were purchased from Rieke Metals Inc. and nano-C Inc., respectively.



IV-2-2. Synthesis of 4-(diphenylamino)benzoic acid (DPA-BA) and 4-(9H-carbazol-9-yl)benzoic acid (Cz-BA)

IV-2-2-1. 4-(diphenylamino)benzaldehyde (1)

A portion of 2.16 g (29.5 mmol) of N,N-dimethyl formamide was added dropwise to a portion of phosphorus oxychloride (4.52 g, 29.5 mmol). The reaction mixture was stirred for 30 minutes at 0 °C. The mixture was added to a solution of triphenylamine (0.48 g, 1.97 mmol) in 10 mL of dichloroethane. Then reaction mixture was stirred for 12 hours at 90 °C. A portion of 100 mL of water was added into the reaction mixture then extracted three times with 50 mL of methylene chloride (MC). The combined organic layer was washed with aqueous sodium carbonate (10 wt.%) and then dried over anhydrous magnesium sulfate (MgSO₄). The solvent was removed using a rotary evaporator. The yield of white crystal was 0.49 g (92.7%). mp: 135.6 °C. ¹H-NMR (400 MHz, CDCl₃, ppm): δ 9.80 (s, 1H), 7.69~7.66 (d, *J* = 11.36 Hz, 2H), 7.35~7.31 (t, *J* = 7.68 Hz, 4H), 7.18~7.15 (m, 6H), 7.03~7.01 (d, *J* = 8.8 Hz, 3H), ¹³C-NMR (100 MHz, CDCl₃, ppm): δ 190.29, 153.23, 146.05, 131.21, 129.65, 129.01, 126.21, 125.02, 119.25. Anal. Calcd. For C₁₉H₁₃NO₂: C, 79.43; H, 4.56; N, 4.88; O, 11.14. Found: C, 79.82; H, 4.51; N, 4.782.

IV-2-2-2. 4-(diphenylamino)benzoic acid (DPA-BA)

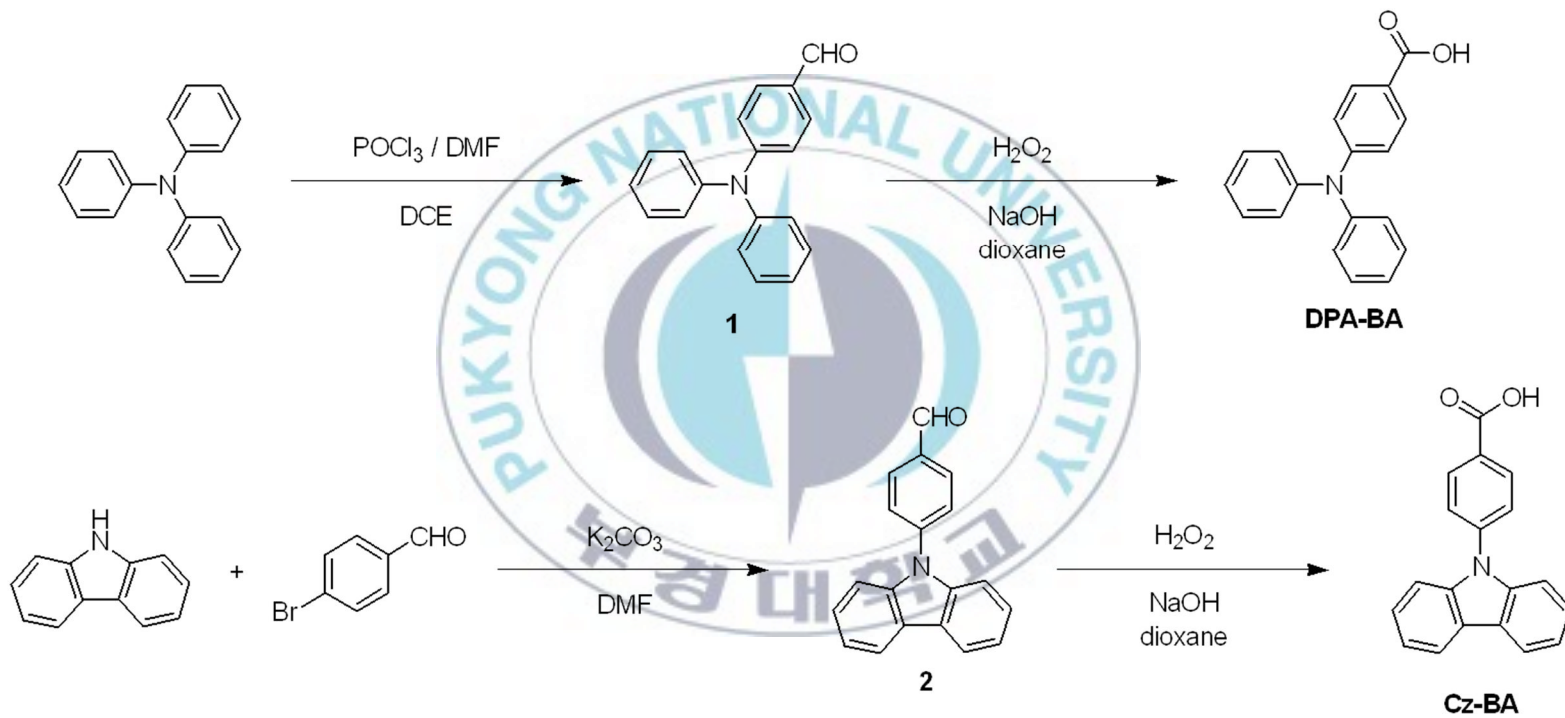
A portion of compound 1 (0.30 g, 1.097 mmol), hydrogen peroxide (2.5 mL, 1.097 mmol) and sodium hydroxide (0.045 g, 1.097 mmol) was dissolved in 5 mL of dioxane and the mixture was stirred for 2 hours at 0 °C. Then the reaction mixture was heated up to 100 °C and stirred for 12 hours. The reaction mixture was cooled down the room temperature and filtered. The filtrate was adjusted to pH 2 with HCl solution, and filtered again. The yield of the gray powder is 0.25 g (78.3 %). mp: 174.9 °C. ¹H-NMR (400 MHz, MeOH-*d*₃, ppm): δ 7.98~7.96 (d, *J* = 8.08 Hz, 2H), 7.33~7.28 (m, 4H), 7.22~7.19 (m, 4H), 7.07~7.02 (t, *J* = 7.32 Hz, 2H), 6.73~6.69 (t, *J* = 8.08 Hz, 2H). Anal. Calcd. For C₁₉H₁₅NO₂: C, 78.87; H, 5.23; N, 4.84; O, 11.06. Found: C, 78.51; H, 5.34; N, 4.69.

IV-2-2-3. 4-(9*H*-carbazol-9-yl)benzaldehyde (2)

A mixture of 4-bromobenzaldehyde (0.231 g, 1.25 mmol), 9*H*-carbazole (0.167 g, 1.00 mmol), copper powder (0.095 g, 1.50 mmol), potassium carbonate (0.207 g, 1.50 mmol) and 18-crown-6 (0.013 g, 0.05 mmol) in 1,2-dichlorobenzene was stirred at 170 °C for 12 hours under the nitrogen atmosphere. After the reaction mixture was cooled down to room temperature, excess of K₂CO₃ and Cu is removed by the filtration. A portion of 100 mL of water was added into the filtrate and then extracted three times of with a portion of 100 mL of MC. The combined organic layer was dried over anhydrous MgSO₄ then the solvent was removed using a rotary evaporator. The yield of the colorless solid was 0.172 g (63.4%). mp: 160.3 °C. ¹H-NMR (400 MHz, CDCl₃, ppm): δ 10.10 (s, 1H), 8.16~8.11 (m, 4H), 7.79~7.77 (d, *J* = 8.08 Hz, 2H), 7.52~7.49 (d, *J* = 8.08 Hz, 2H), 7.46~7.42 (t, *J* = 6.96 Hz, 2H), 7.36~7.32 (t, *J* = 7.72 Hz, 2H), ¹³C-NMR (100 MHz, CDCl₃, ppm): δ 190.92, 143.32, 139.99, 134.56, 131.32, 126.74, 126.23, 123.91, 120.77, 120.45, 109.71. Anal. Calcd. For C₁₉H₁₃NO: C, 84.11; H, 4.83; N, 5.16; O, 5.90. Found: C, 84.10; H, 4.79; N, 5.97.

IV-2-2-4. 4-(9*H*-carbazol-9-yl)benzoic acid (Cz-BA)

A portion of compound 2 (0.061 g, 0.220 mmol), hydrogen peroxide (0.5 mL, 0.220 mmol) and sodium hydroxide (0.009 g, 0.220 mmol) was dissolved in 1 mL of dioxane and the mixture was stirred for 2 hours at 0 °C. Then the reaction mixture was heated up to 100 °C and stirred for 12 hours. The reaction mixture was cooled down the room temperature and filtered. The filtrate was adjusted to pH 2 with HCl solution, and filtered again. The crude residue was recrystallization of n-hexane. The yield of the yellowish white solid is 0.034 g (53.7 %). mp: 213.0 °C. ¹H-NMR (400 MHz, MeOH-*d*₃, ppm): δ 8.31~8.28 (d, *J* = 8.80 Hz, 2H), 8.15~8.13 (d, *J* = 7.68 Hz, 2H), 7.72~7.69 (d, *J* = 8.44 Hz, 2H), 7.47~7.38 (m, 4H), 7.29~7.26 (t, *J* = 7.68 Hz, 2H). Anal. Calcd. For C₁₉H₁₃NO₂: C, 79.43; H, 4.56; N, 4.88; O, 11.14. Found: C, 79.82; H, 4.47; N, 4.79



Scheme 4-1. Synthesis of 4-(diphenylamino)benzoic acid (DPA-BA) and 4-(9H-carbazol-9-yl)benzoic acid (Cz-BA)

IV-2-3. Fabrication of IPSCs

PSCs were fabricated in the configuration of the common sandwich structure: ITO/before and after SAM treated ZnO/active layer/MoO₃/Ag. The ITO-coated glass substrates were cleaned with deionized water, acetone, methanol, 2-propanol in an ultrasonic bath. After the substrates were dried, they were treated with UV/O₃ for 120 seconds prior to use. A layer of 40 nm thick ZnO film was deposited onto the ITO substrate (sheet resistance = 15 Ω/sq) by using sol-gel process. The sol-gel solution was prepared from a mixture of zinc acetate dehydrate (0.164 g) and ethanolamine (0.05 mL) dissolved in 1 mL of methoxyethanol. And then the solution was stirred for 30 min at 60 °C prior to deposition. A layer of 40 nm thick ZnO film was spin-coated on the ITO coated glass and then cured at 300 °C for 10 min to partly crystallize the ZnO film, which is prepared by the literature procedures^{32,43}. Self-assembled molecule was deposited on the ZnO film by spin-coating a 1.0 mg/mL solution of benzoic acid derivative in methanol at 4000 rpm for 60 s. In order to remove physically absorbed molecules, the SAM treated ZnO surface was washed using pure methanol and then dried by the stream of nitrogen. The photoactive layer was formed from 20 mg of P3HT and 20 mg of PCBM blend in 1 mL of o-dichlorobenzene (ODCB) at 600 rpm for 40 s. The sample was then dried in a covered glass petri dish for 1h. Prior to spin coating, the active solution was filtered through a 0.45 μ m membrane filter. The typical thickness of the active

layer was 200 nm. Before the thermal deposition of the MoO₃ buffer and the Ag anode, the sample was thermally annealed at 150 °C for 20 min in the glove box (N₂ atmosphere). Finally, 20 nm thick MoO₃ and 100 nm thick Ag were deposited successively onto the top of the active layer through a shadow mask with a device area of 0.13 cm² at 2×10⁻⁶Torr.



IV-3. Results and Discussion

IV-3-1. Characterization of SAM modified ZnO

To confirm the DPA-BA and Cz-BA treated ZnO, the XPS spectra was measured by SAM. In Figure 4-1, the O 1 s peaks can be de-convoluted into three peaks corresponding to the low binding energy (LP), middle binding energy (MP), and high binding energy (HP) components centered at 530.11, 531.51, and 532.83 eV, respectively⁵⁴. The ZnO crystal lattice peak is located at 530.11 eV (LP) which is attributed to O²⁻ ions surrounded by Zn. At 531.51 eV, the MP is associated with O_x- ions (x < 2) in the oxygen-deficient regions within ZnO matrix and indicated to oxygen vacancies. The HP which is located at 543.83 eV is attributed to chemisorbed oxygen, dissociated oxygen, of OH- groups on the ZnO surface. The oxygen peaks in SAM treated ZnO are shifted to lower binding energy. This result demonstrates that the ZnO (540.62 eV) surface is fully coated by DPA-BA (530.31 eV) and Cz-BA (530.49 eV).

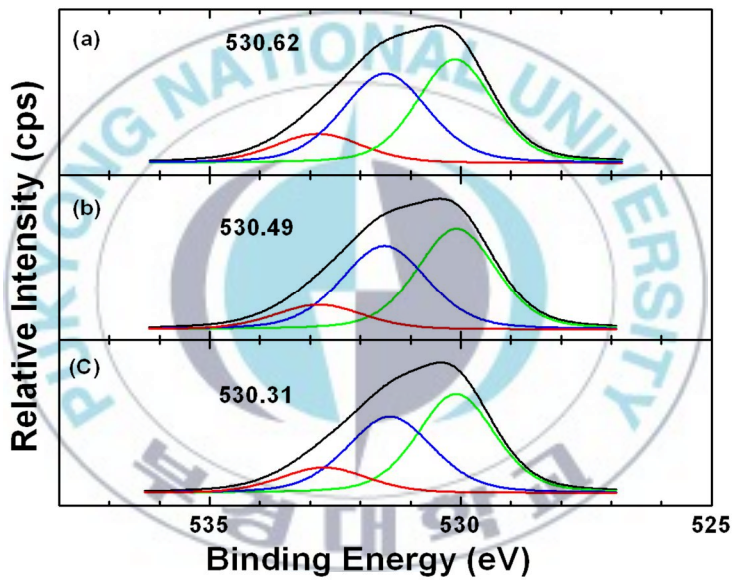
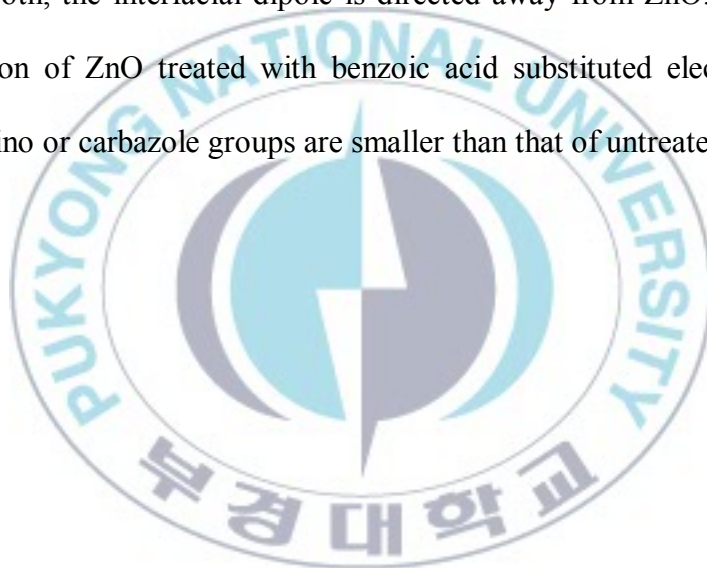


Figure 4-1. XPS Spectra of (a) ZnO, (b) ZnO/DPA-BA and (c) ZnO/Cz-BA

To confirm the effect of SAM treatment on the formation of the interfacial dipole between ZnO and the active layer, we measured by UPS to know the effective work function of ZnO and SAM modified. As shown Figure 4-2, the effective work function of based on ZnO, DPA-BA based on ZnO and Cz-BA based on ZnO are 4.51, 4.42 and 4.35 eV, respectively. The direction of interfacial dipole depends on the permanent dipole orientation of self-assembled molecules. In case of both, the interfacial dipole is directed away from ZnO. The effective work function of ZnO treated with benzoic acid substituted electron donating diphenylamino or carbazole groups are smaller than that of untreated ZnO.



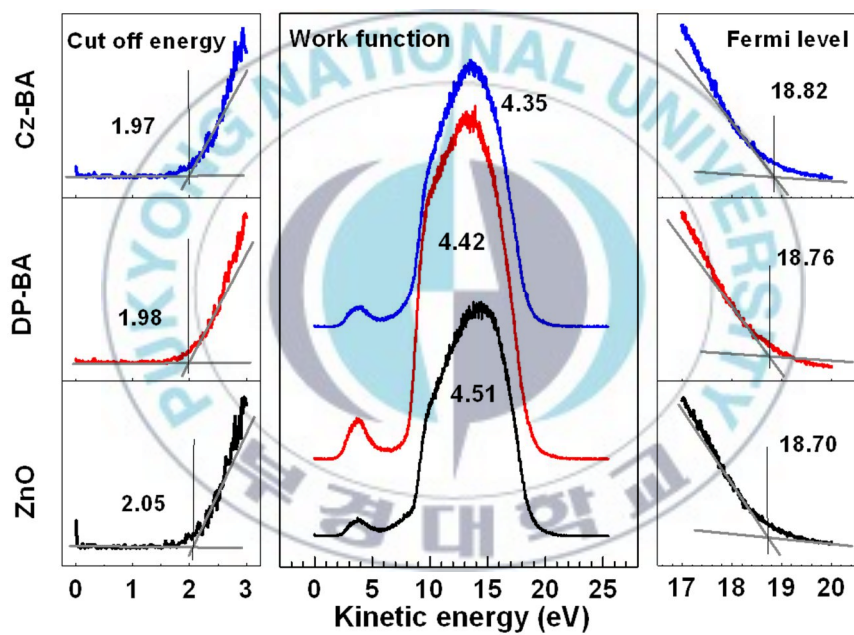


Figure 4-2. UPS spectra of ZnO, ZnO treated DP-BA and Cz-BA.

IV-3-2. Photovoltaic Properties of IPSCs

Figure 4-3 shows the current density-voltage (J-V) curve of IPSCs by using SAM treatment under AM 1.5G simulated illumination with an intensity of 100 mW/cm² and under the dark condition. In Table 1, the resulting photovoltaic parameters and efficiency of the best IPSCs with various SAM based on ZnO are summarized. The V_{oc} of the devices with DPA-BA (0.61 V) and Cz-BA (0.62 V) are higher than that of the devices of without self-assembled molecules (0.60 V). This is attributed by dipole moment made by benzoic acid derivatives anchoring the surface of ZnO in Figure 4-4. Therefore, the effective work function of ZnO/Cz-BA shows the smallest value than the others.

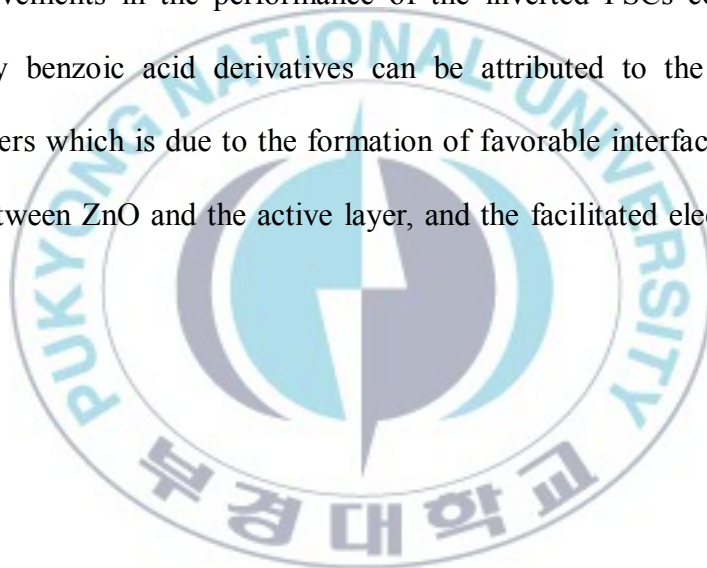
For efficient polymer solar cells, the J_{sc} also is affected the power conversion efficiency. The J_{sc} of the devices with DPA-BA and Cz-BA are -8.34 mA/cm² and -8.29 mA/cm², which is higher than that of the devices based on ZnO (-7.83 mA/cm²). The improved J_{sc} might be ascribed to benzoic acid SAM treatment improving the interfacial electron transfer by removing the trap states at the interface between ZnO layer and the active layer.

The improvement from the DPA-BA and Cz-BA is also observed by the enhanced fill factors. Reducing the hydroxyl groups on the ZnO surface by forming bonds with benzoic acid based SAMs reduces the resistance and recombination losses leading to improvement of fill factors from 53% to 54.6%-56.1% for DPA-BA and Cz-BA treated ZnO, respectively. We can recognize that

device with ZnO/Cz-BA manifests the highest FF. This result demonstrates the good contact between layers of device which possesses the lowest R_s and highest R_p value compared to those of untreated ZnO and ZnO/DPA.

The PCE of the devices using by benzoic acid self-assembled molecules is higher than those of the devices untreated SAM. Table 4-1 shows the PCE of DPA-BA and Cz-BA are 2.78% and 2.88%, which is higher than ZnO (2.49%).

The improvements in the performance of the inverted PSCs containing ZnO modified by benzoic acid derivatives can be attributed to the good contact between layers which is due to the formation of favorable interface dipole at the interface between ZnO and the active layer, and the facilitated electron transport to the ITO.



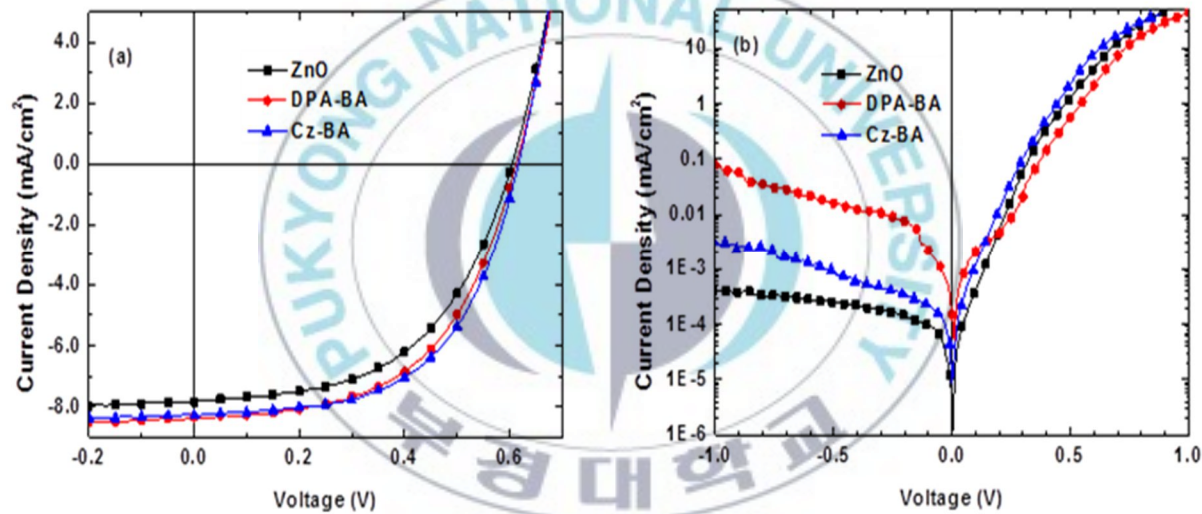


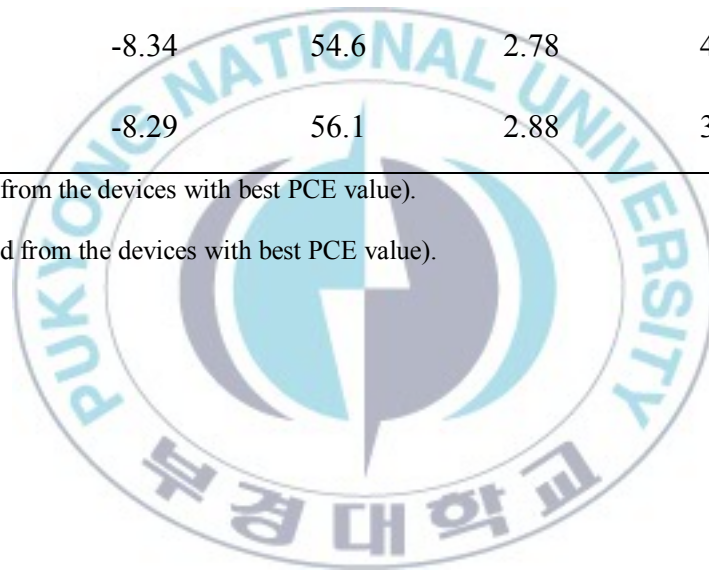
Figure 4-3. Current density-voltage curves of inverted type PSCs (a) under AM 1.5G simulated illumination with intensity of 100 mW/cm² and (b) under the dark condition (square, ZnO; circle, DPA-BA treated ZnO; triangle, Cz-BA treated ZnO).

Table 4-1. Best photovoltaic parameters and efficiencies of PSCs with various SAM treated ZnO.

	V_{oc} (V)	J_{sc} (mA/cm ²)	FF (%)	PCE (%)	R_s ($\Omega \cdot \text{cm}^2$) ^a	R_p ($\text{k}\Omega \cdot \text{cm}^2$) ^b
ZnO	0.60	-7.83	53.0	2.49	6.17	2.45
DPA-BA	0.61	-8.34	54.6	2.78	4.56	23.12
Cz-BA	0.62	-8.29	56.1	2.88	3.07	25.67

^a: series resistnace (estimated from the devices with best PCE value).

^b: paralell resistance (estimated from the devices with best PCE value).



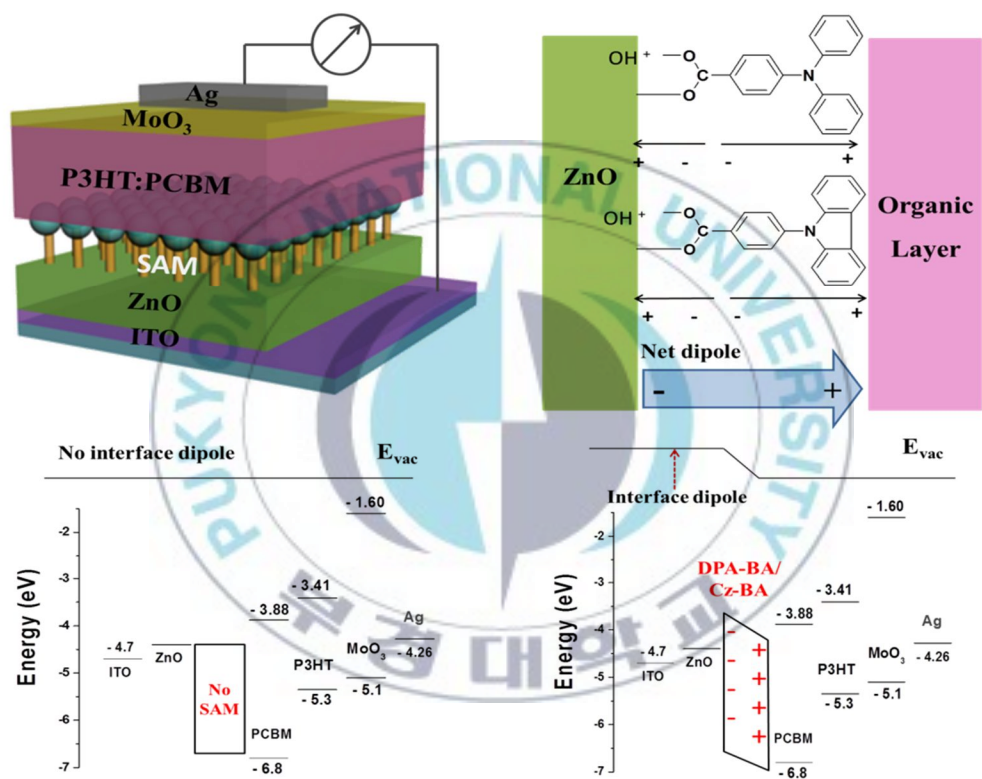


Figure 4-4. Schematic illustration of polymer solar cells with SAM modified ZnO and schematic energy level diagram of the devices with SAM modified ZnO. For ZnO/DPA-BA and ZnO/Cz-BA, the interfacial dipole directed away from ZnO. There is no net interfacial dipole for ZnO without SAM.

IV-3-3. Surface Properties of the Active Layer

In order to the effect of SAM treatment on ZnO surface, we obtained the images of atomic force microscope (AFM). Figure 4-5, the root means square (RMS) roughness of the active layer on DPA-BA (4.13 nm) and Cz-BA (4.35 nm). It was fact that the formation of the active layer with BA SAM treatment more uniform and smooth than without SAM (4.93 nm). Besides, there is no large phase separation, showing good miscibility between P3HT and PCBM.

We investigated the contact angle of each sample to examine the effects of the SAM treatment on the surface properties of the ZnO layer. As shown Figure 4-6., the contact angle values of ZnO, ZnO/DPA-BA and ZnO/Cz-BA are $45.32 \pm 0.61^\circ$, $58.82 \pm 1.04^\circ$ and $60.40 \pm 0.97^\circ$. The increase in contact angle possibly due to hydrophobic characteristic of carbazole and diphenylamine substituted benzoate. We confirmed that ZnO surface with SAMs based on benzoic acid derivatives were fabricated successfully on the ZnO layer from the contact angle data.

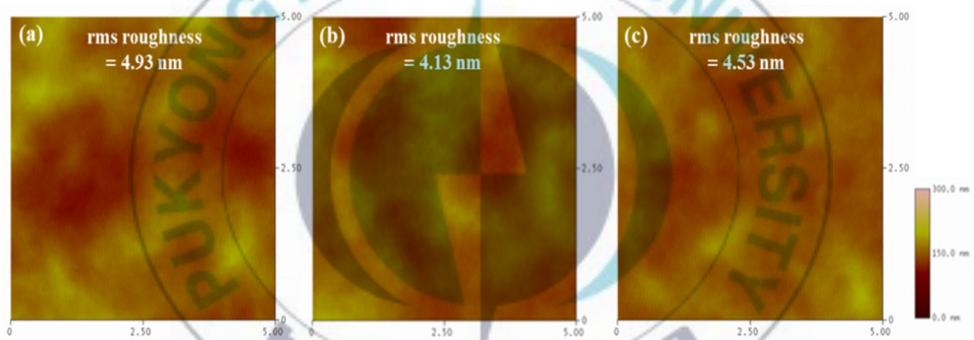


Figure 4-5. AFM topography images of thermally annealed P3HT/PCBM film on (a) ZnO, (b) ZnO/ DPA-BA, and (c) ZnO/Cz-BA (x, y = 1 $\mu\text{m}/\text{div.}$, z = 100 nm/div.).

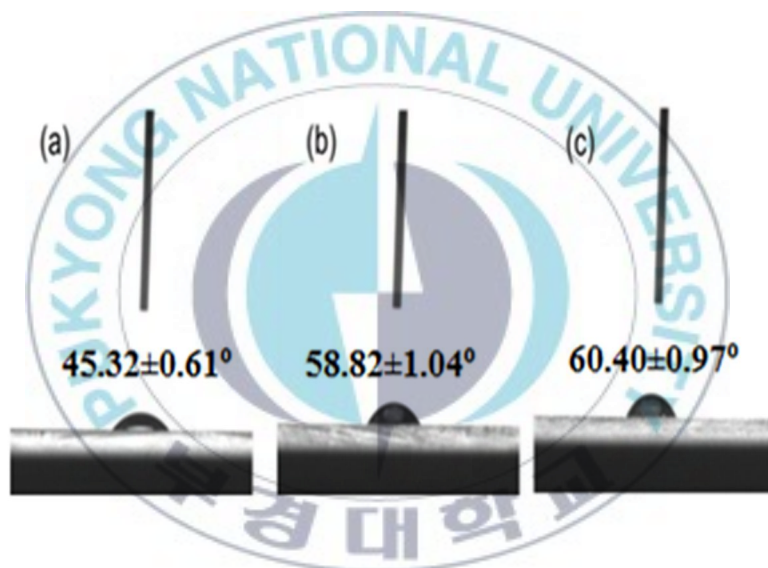


Figure 4-6. Photographs from water contact angle measurements on (a) ZnO, (b) DPA-BA treated ZnO, and (c) Cz-BA treated ZnO.

IV-4. Conclusion

We have demonstrated the highly efficient inverted polymer solar cells by using solution-processed ZnO treated SAMs as cathode buffer layers. The results showed that thanks to benzoic acid based SAMs on ZnO, the favorable interface dipole was formed by removing the trap states at the interface of the ZnO layer. The facilitation in electron transport from active layer to the ITO electrode led to improve performances of devices with ZnO treated SAMs. The IPSC based on CZ-BA modified ZnO showed the best performances with V_{oc} of 0.62 V, J_{sc} of -8.29 mA/cm², FF of 56.1% and PCE of 2.88%. In addition, the performances of the device with benzoic acid derived from aryl-benzoic acid derivatives treated ZnO poorer than those of the device with alkyl-benzoic acid derivatives treated ZnO (in chapter III).

Chapter V. Conventional type Polymer Solar Cells and Polymer Light Emitting Diodes Using Non-conjugated Polymer with Polar Group as Electron Transporting Materials

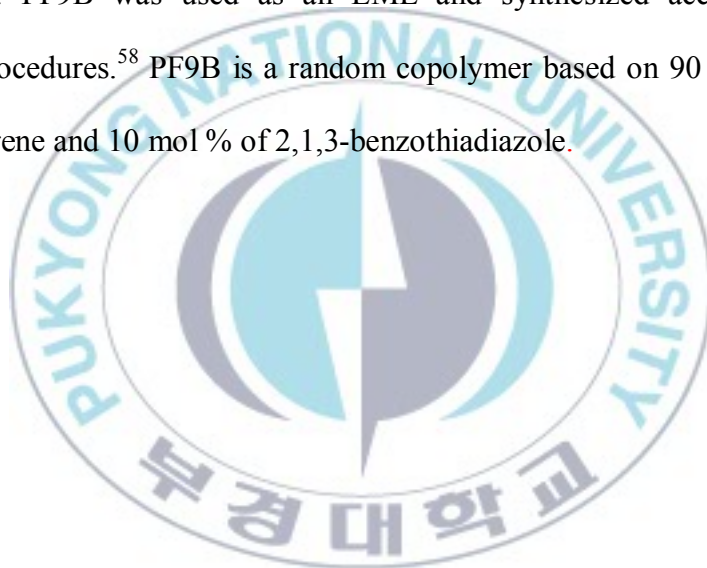
V-1. Introduction

Recently, the organic optoelectronic devices, such as polymer light-emitting diodes (PLEDs) and polymer solar cells (PSCs), have been studied because of low fabrication cost and the possibility of their application in flexible devices.^{1,2,55,56} One of important factors is the charge transporting and injecting/collecting properties for influencing the performances of the devices. These are strongly related to the interfacial properties between the emissive layer (or the active layer) and the electrodes.⁵⁷ To improve interfacial property, one of many methods is the insertion of a buffer layer between the emitting layer (or the active layer) and the metal electrode. A non-conjugated anionic polymer, such as poly(vinyl alcohol) (PVA), might be used as an electron injection layer (EIL) between the emitting layer (or the active layer) and the cathode. PVA is a well-known commercially available non-conjugated polymer with polar group and very good soluble in polar protic solvents, such as water or water/alcohol mixtures. We investigated the effect of PVA with polar group as EIL of ETL in PLEDs and conventional PSCs.

V-2. Experiment Section

V-2-1. Materials

Chemicals were purchased from Aldrich Chemical Co. and Alfa Aesar and were used as received unless otherwise described. Poly vinyl alcohol, 98-99% hydrolyzed, high molecular weight was purchased from Alfa Aesar. Regioregular P3HT and PCBM were purchased from Rieke Metals Inc. and nano-C, Inc., respectively. PF9B was used as an EML and synthesized according to the literature procedures.⁵⁸ PF9B is a random copolymer based on 90 mol % of 9,9-dihexylfluorene and 10 mol % of 2,1,3-benzothiadiazole.



V-2-2. Fabrication of CPSCs

For fabrication of PSCs with a structure of ITO/PEDOT:PSS/P3HT:PCBM/PVA/Al. After being baked at 150 °C for 10 min under the air of a PEDOT (Baytron P, diluted with 2-propanol 1:2 v/v) layer, the active layer was spin-cast from the blend solution of P3HT and PCBM (20 mg of P3HT and 20mg of PCBM dissolved in 1.0 mL of o-dichlorobenzene (ODCB)) at 600 rpm for 40 s and then dried in a covered Petri dish for 1 h. Prior to spin-coating, the photoactive solution was filtered through a 0.45 µm membrane filter. The typical thickness of the active layer was 200 nm. Before cathode deposition, the electron transporting layer (ETL) of PVA was prepared by spin-coating with a different concentration (0.2, 0.5 and 1.0 mg/mL) of PVA and solvent (H₂O/MeOH and DMSO/MeOH 5:95 by volume) at 4000 rpm for 60 s. The Al layer was deposited with a thickness of 100 nm through a shadow mask with a device area of 0.13 cm² at 2×10^{-6} Torr. After the cathode deposition, the device was thermally annealed at 160 °C for 10 min in the glove box (N₂ atmosphere).

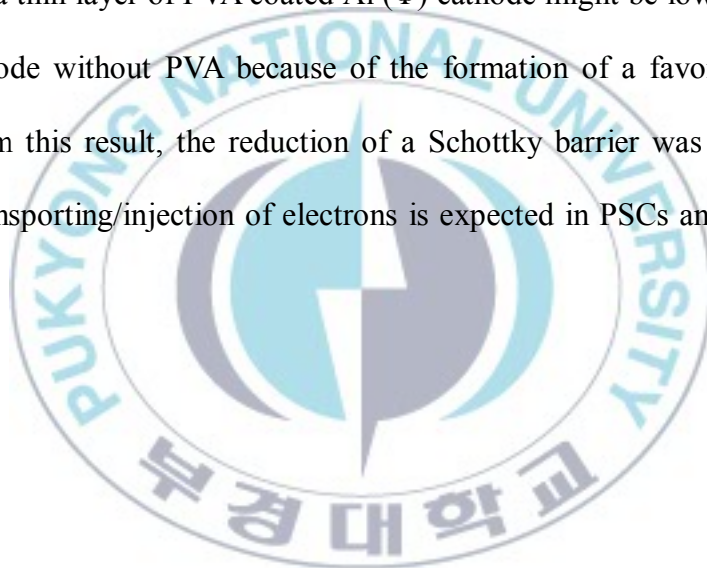
V-2-3. Fabrication of PLEDs

For fabrication of PLEDs with a structure of ITO/PEDOT/PF9B/PVA/Al, a thickness of 40 nm of PEDOT AI 4083 was spin-coated on a pre-cleaned indium tin oxide (ITO) glass substrate (sheet resistance = 15 ohm/sq). After being baked at 150 °C for 10 min under the air, an emissive polymer solution (10 mg/mL in toluene) was spin-coated onto the PEDOT AI 4083 layer at 2000 rpm for 60 s. Before spin-coating, the emissive polymer solution was filtered through a 0.45 μm membrane filter. The typical thickness of an emitting layer was 60 nm. Before cathode deposition, the electron injection layer (EIL) of PVA was prepared by spin-coating with a different concentration (0.2, 0.5 and 1.0 mg/mL) of PVA and solvent (H₂O/MeOH and DMSO/MeOH 5:95 by volume) at 4000 rpm for 60 s. The typical thickness of a PVA film was less than 5 nm. The thickness of the PVA layer was controlled by the concentration and mixed solvent (H₂O/MeOH and DMSO/MeOH) of the PVA solution. The Al layer was deposited with a thickness of 100 nm through a shadow mask with a device area of 0.13 cm² at 2×10^{-6} Torr.

V-3. Results and Discussion

V-3-1. Characterization of CPSCs and PLEDs with Poly(vinyl alcohol)

To confirm the effect the interfacial dipole between active layer and metal surface, we measured by ultra photoelectron spectrometer (UPS) to know the effective work function by polar groups. As shown Figure 5-1, the effective work function of Al and PVA treated Al is 4.43 and 4.30 eV, respectively. The work function of a thin layer of PVA coated Al (Φ) cathode might be lower than that of the Al cathode without PVA because of the formation of a favorable interface dipole. From this result, the reduction of a Schottky barrier was small and the efficient transporting/injection of electrons is expected in PSCs and PLEDs with PVA.



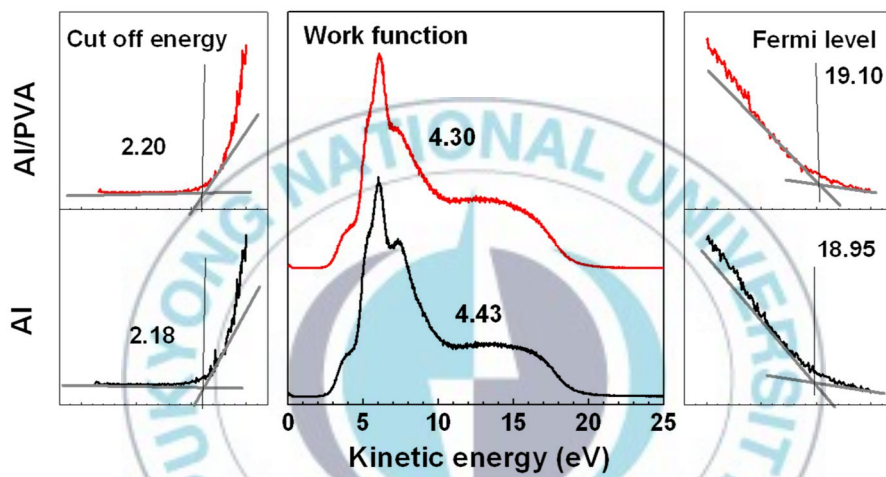


Figure 5-1. UPS spectra of PVA treated Al and ITO.

V-3-2. Photovoltaic Properties of CPSCs

Figure 5-2 show CPSCs configuration made by two type of solvent and various concentration, which is ITO/PEDOT:PSS/P3HT:PCBM/PVA/Al. The J-V curve of CPSCs with PVA as an electron transporting layer shows in Figure 5-3 and the photovoltaic parameters are summarized in Table 5-1 under AM 1.5G simulated illumination with an intensity of 100 mW/cm^2 and under the dark condition.

The V_{oc} of the devices with concentration of 0.2 mg/mL PVA in $\text{H}_2\text{O/MeOH}$ (0.61 V), 0.2 mg/mL (0.63 V), 0.5 mg/mL (0.63 V) and 1.0 mg/mL (0.63 V) PVA in DMSO/MeOH are higher than that of the devices of electron transporting layer (0.59 V). This is attributed to the reduction of a Schottky barrier is small. Therefore, the effective work function of Al/PVA shows the smallest value than the others. Short circuit current (J_{sc}) data of the devices are -7.64 mA/cm^2 (without PVA), -7.98 mA/cm^2 (0.2 PVA in $\text{H}_2\text{O/MeOH}$), -8.28 mA/cm^2 (0.5 PVA in $\text{H}_2\text{O/MeOH}$), -8.21 mA/cm^2 (0.2 PVA DMSO/MeOH), -8.33 mA/cm^2 (0.5 PVA in DMSO/MeOH) and -8.70 mA/cm^2 (1.0 PVA in DMSO/MeOH), respectively. The device with PVA shows better J_{sc} than that of the device without PVA. The fill factor (FF) data of the device with concentration of 0.2 mg/mL, 0.5 mg/mL PVA in $\text{H}_2\text{O/MeOH}$, 0.2 mg/mL, 0.5 mg/mL and 1.0 mg/mL PVA in DMSO/MeOH are 55.4%, 54.6%, 59.9%, 60.4%, and 59.7%, which is also higher than that of the device untreated PVA (54.1%). This is a result related to the lowest R_s and highest R_p value compared to that of device without PVA. We also

confirm that the effect of PVA interfacial layer with electron injection ability and DMSO/MeOH is the good solvent to resolve PVA. The best power conversion efficiency (PCE) of the devices with concentration of 1.0 mg/mL PVA in DMSO/MeOH was 3.27% which is a 34% increase compare to that of the device without PVA. These result indicate that the effect of the PVA cathode buffer layer is dependent on solvent.

Figure 5-4 shows the maximum of incident photon to collected electron efficiency (IPCE) of the IPSC at 545 nm. The device with concentration of 1.0 mg/mL PVA in DMSO/MeOH shows the highest value (67.4%), which is higher than that of the device without PVA (62.5%), with concentration of 0.2 mg/mL PVA on DMSO/MeOH (64.5%) and 0.5 mg/mL in PVA in DMSO/MeOH (65.0%). The IPCE also demonstrate the photovoltaic parameters are related to the performances of IPSCs with PVA treated P3HT:PCBM.

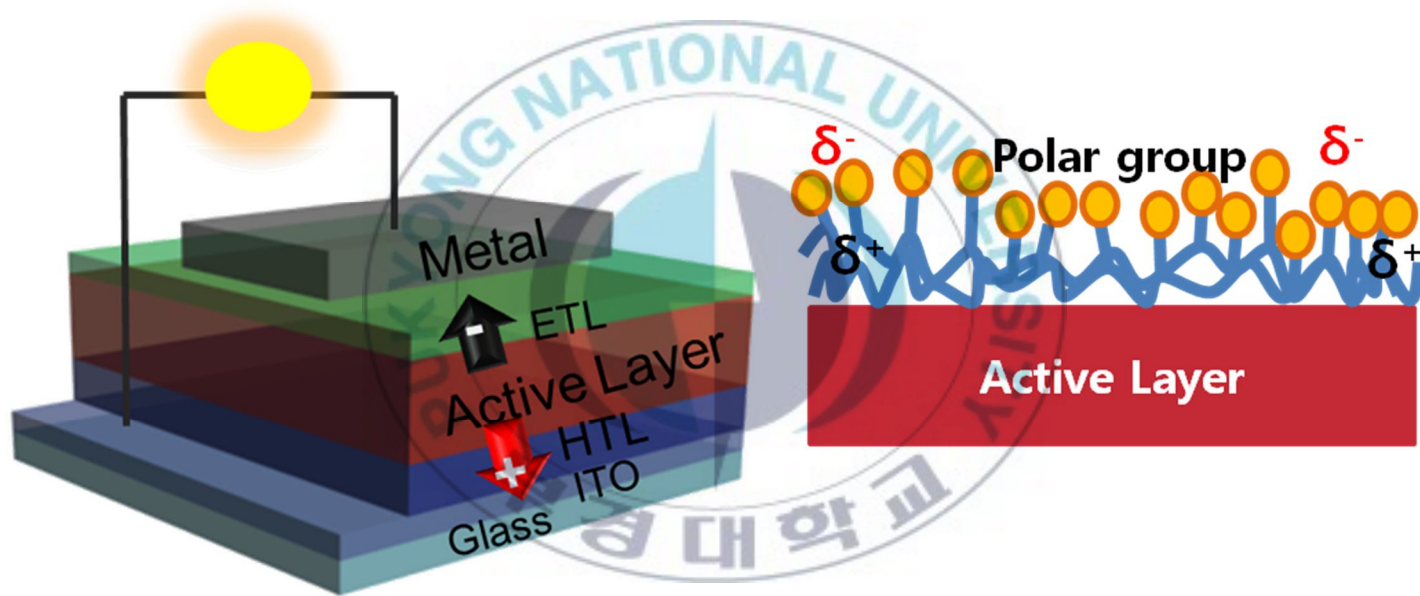


Figure 5-2. Structure of CPSCs with PVA.

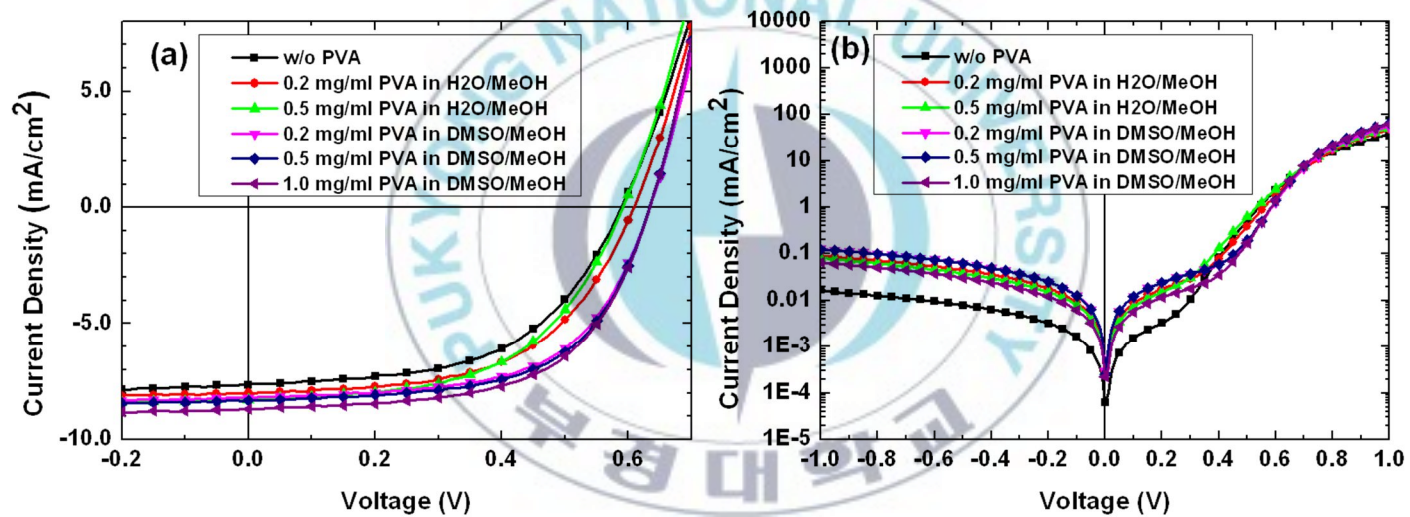


Figure 5-3. Current density-voltage curves of CPSCs (a) under AM 1.5G simulated illumination with an intensity of 100 mW/cm² and (b) under the dark condition

Table 5-1. The best photovoltaic parameters and efficiencies of CPSCs with PVA. The averages for photovoltaic parameters of each device are given in parentheses with mean variation.

Solvent	Concentration	V_{oc} (V)	J_{sc} (mA/cm ²)	FF (%)	PCE (%)	$R_s(\Omega \cdot \text{cm}^2)^a$	$R_p(\text{k}\Omega \cdot \text{cm}^2)^b$
H ₂ O/MeOH	w/o PVA	0.59 (0.59 ± 0.01)	-7.64 (-7.59 ± 0.21)	54.1 (54.5 ± 1.67)	2.44 (2.43 ± 0.05)	5.75	61.84
	0.2 mg/mL	0.61 (0.61 ± 0.00)	-7.98 (-8.02 ± 0.05)	55.4 (55.0 ± 0.40)	2.70 (2.70 ± 0.01)	3.14	11.05
	0.5 mg/mL	0.59 (0.59 ± 0.00)	-8.28 (-8.27 ± 0.02)	54.6 (54.1 ± 0.50)	2.67 (2.64 ± 0.03)	2.98	12.36
DMSO/MeOH	0.2 mg/mL	0.63 (0.63 ± 0.01)	-8.21 (-8.04 ± 0.15)	59.9 (59.4 ± 0.64)	3.10 (3.01 ± 0.04)	2.78	7.84
	0.5 mg/mL	0.63 (0.64 ± 0.01)	-8.33 (-8.12 ± 0.18)	60.4 (59.4 ± 0.05)	3.17 (3.06 ± 0.05)	2.46	7.97
	1.0 mg/mL	0.63 (0.64 ± 0.01)	-8.70 (-8.36 ± 0.24)	59.7 (59.3 ± 0.93)	3.27 (3.15 ± 0.06)	2.72	15.31

^a: series resistnace (estimated from the devices with best PCE value). ^b: parallll resistance (estimated from the devices with best PCE value).

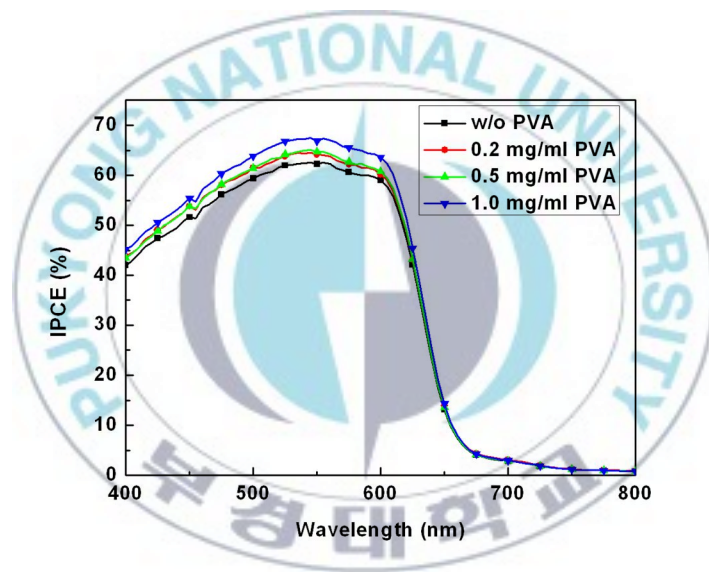


Figure 5-4. IPCE Spectra of CPSCs with PVA in DMSO/MeOH solution.

V-3-3. Luminescent Properties of PLEDs

In order to investigate the effect of non-conjugated polymer, we fabricated PLEDs with PVA mixed-solution using DMSO/MeOH as electron injection layer (EIL) in Figure 5-5. The Figure 5-6, 5-7 and Table 5-2 show the characteristic and performances of PLEDs with or without EIL. As shown Figure 5-6, the device with the PVA as an EIL exhibited better than electron transporting ability than that of the devices without EIL. The device without PVA showed a turn-on voltage (V_{on}) of 9.5 V, the maximum luminance efficiency (LE_{max}) of 1.16 cd/A, and a maximum brightness (B_{max}) of 3968 cd/m², respectively. On the contrary, the device with concentration of 1.0 mg/mL PVA in DMSO/MeOH showed a turn-on voltage (V_{on}) of 7.0 V, the maximum luminance efficiency (LE_{max}) of 3.61 cd/A, and a maximum brightness (B_{max}) of 2249 cd/m² in Figure 5-5, 5-6 and Table 5-2. One of reason for the poor B_{max} is not fully covered with the PVA. And the V_{on} values of the devices with the PVA film were smaller than that of the device without PVA, indicating that the electron injection process is facilitated by the PVA. The electron injection properties are improved by PVA between the emitting layer and the cathode, even though the reduction of a Schottky barrier was small.

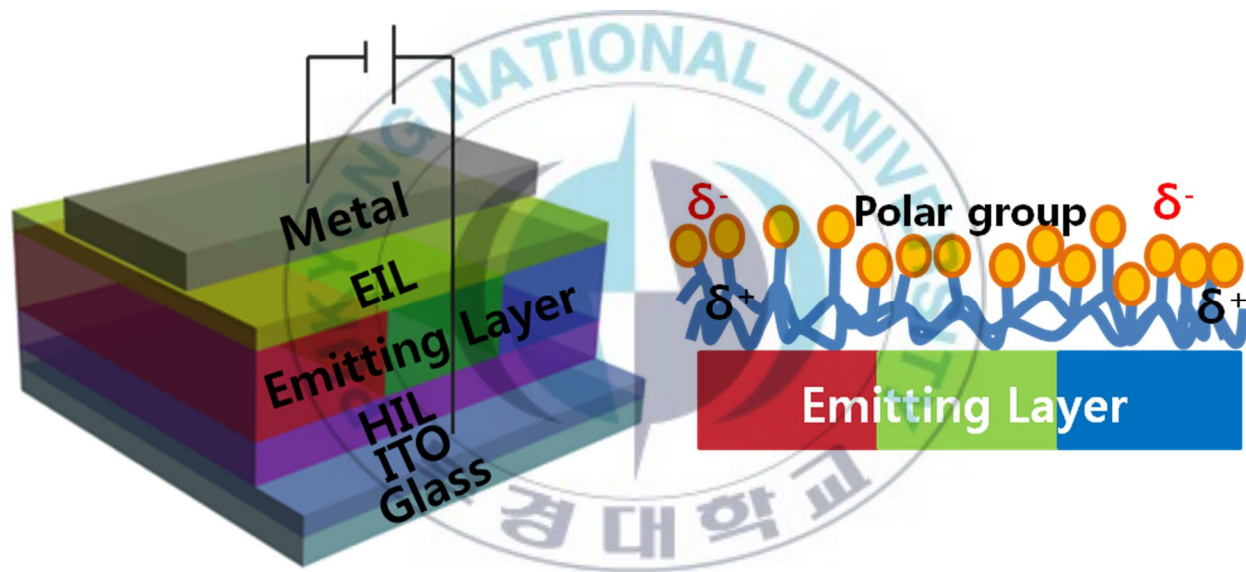


Figure 5-5. Structure of PLEDs with PVA.

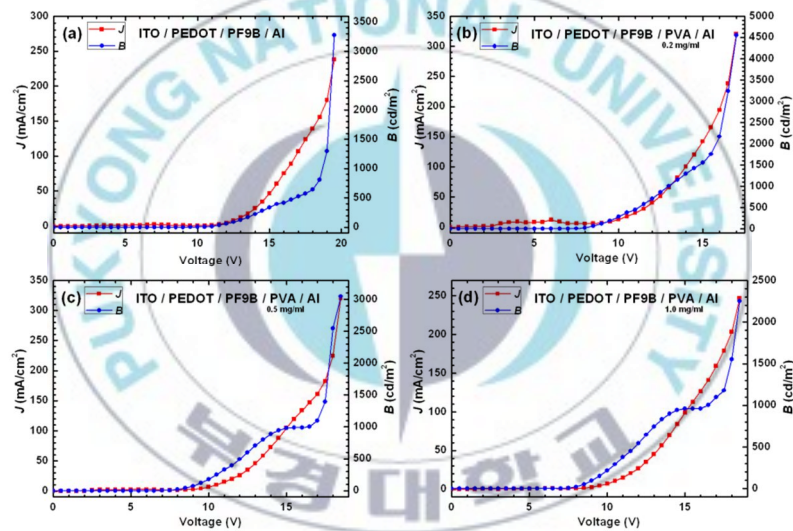


Figure 5-6. Current density-Voltage-Brightness spectra of PLEDs (a) without PVA, (b) with PVA of 0.2 mg/mL, (c) with PVA of 0.5 mg/mL and (d) with PVA of 1.0 mg/mL

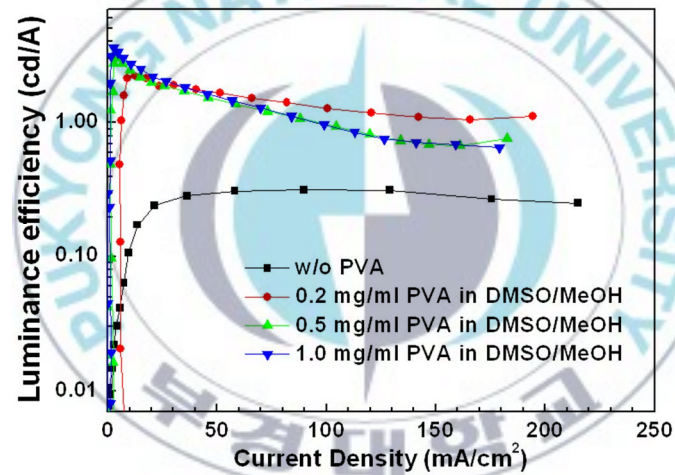


Figure 5-7. Luminance efficiency spectra of PLEDs without PVA and with PVA.

Table 5-2. Performance of PLEDs with PVA in DMSO/MeOH.

	V_{on}^a (V)	LE_{max}^b (cd/A)	LE_{100}^c (cd/A)	B_{max}^d (cd/m ²)
Without PVA	9.5	1.157 (at 16.5 mA/cm ²)	0.29	3968
0.2 mg/mL PVA	7.0	2.220 (at 9.0 mA/cm ²)	1.60	4558
0.5 mg/mL PVA	7.0	3.018 (at 9.0 mA/cm ²)	3.02	3050
1.0 mg/mL PVA	7.0	3.612 (at 10 mA/cm ²)	3.61	2249

^aTurn-on voltage is defined as the voltage at a brightness of 1 cd/m².

^bMaximum luminance efficiency.

^cLuminance efficiency at a brightness of 100 cd/m².

^dMaximum brightness.

V-3-4. Surface Properties of the Active Layer

To investigate the effect of the EIL on the surface properties of active layer, we measured the surface energy by using water and di-iodomethane in Figure 5-8 and Table 5-3. Without PVA as EIL, the active layer showed the surface energy 23.57 mN/m. Whereas, the contact angle with PVA of 0.2 mg/mL in H₂O/MeOH, 0.5 mg/mL in H₂O/MeOH, 0.2 mg/mL in DMSO/MeOH, 0.5 mg/mL in DMSO/MeOH and 1.0 mg/mL in DMSO/MeOH are 23.99 mN/m, 23.64 mN/m, 27.24 mN/m, 26.80 mN/m and 26.80 mN/m, respectively. The decrease of surface energy is attributed to hydrophilic characteristic of PVA with polar group. As shown Figure 5-9, we also obtained AFM images to confirm the morphology of the active layer. The roughness means square (RMS) of the device without PVA is 3.45 nm, which is harsher than that of device with PVA. This result indicated that the PVA solution coated uniform on the active layer.



Figure 5-8. Water contact angle of films (a) without PVA, (b) with PVA of 0.2 mg/mL in H₂O/MeOH, (c) with PVA of 0.5 mg/mL in H₂O/MeOH, (d) with PVA of 0.2 mg/mL in DMSO/MeOH (e) with PVA of 0.5 mg/mL in DMSO/MeOH and (f) with PVA of 1.0 mg/mL in DMSO/MeOH

Table 5-3. Contact angle and calculated surface energy of film without or with PVA.

	Without PVA	0.2 mg/mL PVA H ₂ O/MeOH	0.5 mg/mL PVA H ₂ O/MeOH	0.2 mg/mL PVA DMSO/MeOH	0.5 mg/mL PVA DMSO/MeOH	1.0 mg/mL PVA DMSO/MeOH
Drop H ₂ O (°)	107.09	106.24	106.16	104.83	104.12	104.02
Drop DIM (°)	69.56	68.66	69.19	63.32	63.87	63.91
γ^d ^a (mN/m)	23.43	23.81	23.43	27.14	26.62	26.62
γ^p ^b (mN/m)	0.14	0.18	0.21	0.1	0.18	0.18
γ^c (mN/m)	23.57	23.99	23.64	27.24	26.80	26.80

^a: dispersion term of surface energy ^b: polar term of surface energy ^c: total of surface energy

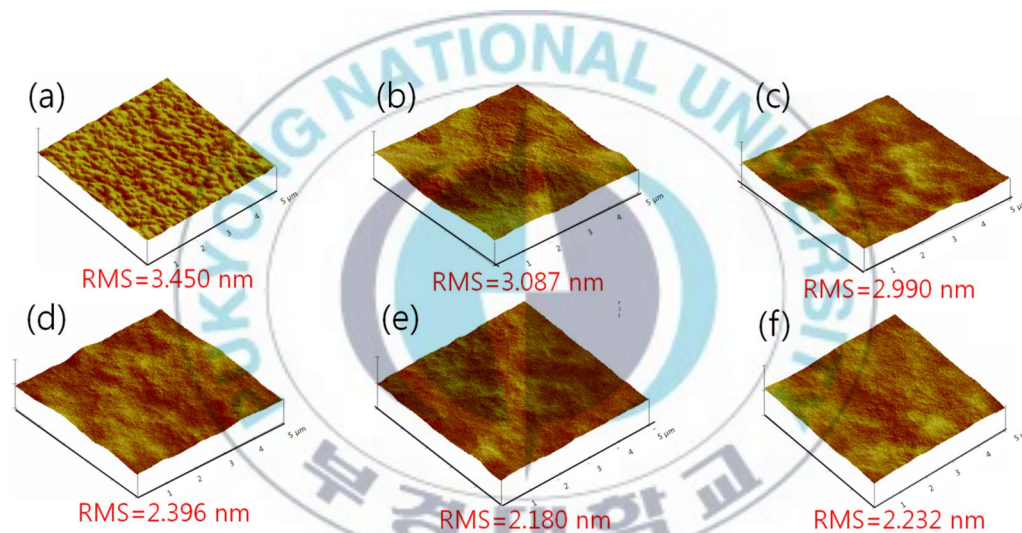
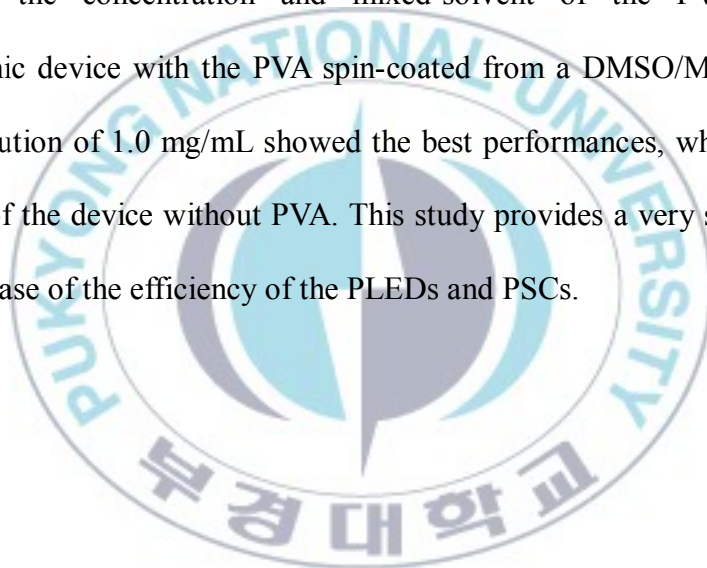


Figure 5-9. AFM images of the device (a) without PVA, (b) with PVA of 0.2 mg/mL in H₂O/MeOH, (c) with PVA of 0.5 mg/mL in H₂O/MeOH, (d) with PVA of 0.2 mg/mL in DMSO/MeOH (e) with PVA of 0.5 mg/mL in DMSO/MeOH and (f) with PVA of 1.0 mg/mL in DMSO/MeOH

V-4. Conclusion

We have confirmed an anionic non-conjugated polymer, which is PVA, to modify the property at the active or emitting layer/Al interface in both PLEDs and PSCs. The UPS results demonstrated that a Schottky barrier between the active or emitting layer and the Al cathode is reduced by the formation of a proper interface dipole by the thin PVA. The performances of PLEDs and PSCs depend on the concentration and mixed-solvent of the PVA film. The optoelectronic device with the PVA spin-coated from a DMSO/MeOH (5:95 by volume) solution of 1.0 mg/mL showed the best performances, which are higher than those of the device without PVA. This study provides a very simple method for the increase of the efficiency of the PLEDs and PSCs.



References

- [1] G. Yu, J. Gao, J. C. Hummelen, F. Wudl, A. J. Heeger, (1995) *Science*, **270**, 1789-1791.
- [2] S. Gunes, H. Neugebauer, N. S. Sariciftci, (2007) *Chem. Rev.*, **107**, 1324-1338.
- [3] B. C. Thompson, J. M. J. Fréchet, (2008) *Angew. Chem., Int. Ed.*, **47**, 58-77.
- [4] G. Dennler, M. C. Scharber, C. J. Brabec, (2009) *Adv. Mater.* **21**, 1323-1338.
- [5] F. C. Krebs, J. Fyenbo, M. Jørgensen, (2010) *J. Mater. Chem.* **20**, 8994-9001.
- [6] C. Deibel, V. Dyakonov, (2010) *Rep. Prog. Phys.* **73**, 096401–1-39.
- [7] W. Z. Cai, X. Gong, Y. Cao, (2010) *Solar Energy Mater. Solar Cells*, **94**, 114–127.
- [8] Y. J. He, Y. F. Li, (2011) *Phys. Chem. Chem. Phys.* **13**, 1970–1983.
- [9] S. E. Shaheen, C. J. Barbec, N. S. Scriciftci, F. Padinger, T. Fromherz, J. C. Hummelen, (2001) *Appl. Phys. Lett.* **78**, 841–843.
- [10] G. Li, V. Shrotriya, J. Huang, Y. Yao, T. Moriarty, K. Emery, Y. Yang, (2005) *Nat. Mater.* **4**, 864–868.
- [11] W. Ma, C. Yang, X. Gong, K. Lee, A. J. Heeger, (2005) *Adv. Funct. Mater.* **15**, 1617–1622.
- [12] M. T. Dang, L. Hirsch, G. Wantz, (2011) *Adv. Mater.* **23**, 3597–3602.
- [13] T. C. Monson, M. T. Lloyd, D. C. Olson, Y.-J. Lee, J. W. P. Hsu, (2008) *Adv. Mater.* **20**, 4755–4759.

- [14] C. J. Brabec, S. E. Shaheen, C. Winder, N. S. Sariciftci, P. Denk, (2002) *Appl. Phys. Lett.* **80**, 1288–1290.
- [15] S. Hau, H. Yip, O. Acton, N. S. Baek, H. Ma, A. K. Y. Jen, (2008) *J. Mater. Chem.* **18**, 5113–5119.
- [16] S. C. Veenstra, A. Heeres, G. Hadziioannou, G. A.; Sawatzky, H. Y. Jonkman, (2002) *Appl. Phys. A: Mater. Sci. Process.* **75**, 661–666.
- [17] H. Choi, J. S. Park, E. Jeong, G. -W. Kim, B. R. Lee, S. O. Kim, M. H. Song, H. Y. Woo, (2011) *J. Adv. Mater.* **23**, 2759–2763
- [18] F. Zhang, M. Ceder, O. Inganäs, (2007) *Adv. Mater.* **19**, 1835–1838.
- [19] V. De Renzi, R. D. Rousseau, D. Marchetto, R. Biagi, S. Scandolo, U. del Pennino, (2005) *Phys. Rev. Lett.* **95**, 046804.
- [20] M. Y. Jo, Y. E. Ha, J. H. Kim, (2012) *Sol. Energy Mater. Sol. Cells*, **107**, 1–8.
- [21] M. Y. Jo, Y. E. Ha, J. H. Kim, (2013) *Organic Electronics*, **14**, 995–1001.
- [22] Y.-J. Cheng, S.-H. Yang, C.-S. Hsu, (2009) *Chem. Rev. (Washington, DC, U. S.)*, **109** (11), 5868–5923.
- [23] J. Chen, Y. Cao, (2009) *Acc. Chem. Res.* **42** (11), 1709–1718.
- [24] M. Lenes, G.-J. A. H. Wetzelaer, F. B. Kooistra, S. C. Veenstra, J. C. Hummelen, P. W. M. Blom, (2008) *Adv. Mater.* **20** (11), 2116 – 2119.
- [25] Y. He, H.-Y. Chen, J. Hou, Y. J. Li, (2010) *Am. Chem. Soc.* **132** (4), 1377–1382.
- [26] G. Zhao, Y. He, Y. Li, (2010) *Adv. Mater.* **22** (39), 4355–4358.

- [27] S. H. Oh, S. I. Na, J. Jo, B. Lim, D. J. Vak, D. Y. Kim (2010) *Adv. Funct. Mater.* **20**, 1977–1983.
- [28] G. E. Lim, Y. E. Ha, M. Y. Jo, J. Y. Park, Y. C. Kang, J. H. Kim (2013) *ACS Appl. Mater. Interfaces.* **5**, 6508–6513.
- [29] F. L. Zhang, M. Johansson, M. R. Andersson, J. C. Hummelen, O. Inganas, (2012) *Adv. Mater.* **14**, 662–665.
- [30] D.C. Look (2001) *Materials Science and Engineering*, **B80**, 383–387.
- [31] J. E. B. Waldo, M. W. Martijn, K. Martijn, Y. Xiaoni, A. J. J. Rene (2005) *J. Phys. Chem. B* **109**, 9505-9516.
- [31] -L. Y. Hin, K. H. Steven, N. S. Baek, A. K. Y. Jen (2008) *Appl. Phys. Lett.*, **92**, 193313.
- [32] H. O. Seo, S. Y. Park, W. H. Shim, K. D. Kim, K. H. Lee, M. Y. Jo, J. H. Kim, E. Lee, D. W. Kim, Y. D. Kim, D. C. Lim (2011) *J. Phys. Chem. C* **115**, 21517–21520.
- [33] W. Lingna, M. J. Mamoun (1999) *Mater. Chem.*, **9**, 2871-2878.
- [34] H. Liu, W. P. Goh, M. Y. Leung, Y. Li, T. B. Norsten (2012) *Solar Energy Materials & Solar Cells* **96**, 302–306.
- [35] J. K. Lee, W. L. Ma, C. J. Brabec, J. Yuen, J. S. Moon, J. Y. Kim, K. Lee, G. C. Bazan, A. J. Heeger (2008) *J. Am. Chem. Soc.* **130**, 3619.
- [36] A. J. Moule', K. Meerholz (2008) *Adv. Mater.* **20**, 240.

- [37] S. Khodabakhsh, B. M. Sanderson, J. Nelson, T. S. Jones (2006) *Adv. Funct. Mater.* **16**, 95.
- [38] C. Goh, S. R. Scully, M. D. McGehee (2007) *J. Appl. Phys.* **101**, 114503.
- [39] T. C. Monson, M. T. Lloyd, D. C. Olson, Y. -J. Lee, J. W. P. Hsu (2008) *Adv. Mater* **20** , 4755.
- [40] S. Hau, H. Yip, O. Acton, N. Baek, H. Ma, A. K. Y. Jen, (2008) *J. Mater. Chem.* **18**, 5113.
- [41] Y. E. Ha, M. Y. Jo, J. Y. Park, Y. C. Kang, S. I. Yoo, J. H. Kim (2013) *J. Phys. Chem. C*, **117**, 2646–2652.
- [42] S. Hau, H. Yip, H. Ma, A. K. Y. Jen (2008) *Appl. Phys. Lett.* **93**, 233304.
- [43] X. Bulliard, S. -G. Ihn, S. Yun, Y. Kim, D. Choi, J. -Y. Choi, M. Kim, M. Sim, J. -H. Park, W. Choi, et al. (2010) *Adv. Funct. Mater.* **20**, 4381–4387.
- [44] A. Hayakawa, O. Yoshikawa, T. Fujieda, K. Uehara, S. Yoshikawa (2007) *Appl. Phys. Lett.* **90**, 163517–1–163517–3.
- [45] J. Y. Kim, S. H. Kim, H. H. Lee, K. Lee, W. Ma, X. Gong, A. J. Heeger (2006) *Adv. Mater* **18**, 572–576.
- [46] K. Lee, J. Y. Kim, S. H. Park, S. H. Kim, S. Cho, A. J. Heeger (2007) *Adv. Mater.* **19**, 2445–2449.
- [47] M. C. Scharber, D. Muhlbacher, M. Koppe, P. Denk, C. Waldauf, A. J. Heeger, C. J. Brabec (2006) *Adv. Mater.* **18**, 789–794.

- [48] A. L. Roest, J. J. Kelly, D. Vanmaekelbergh, E. A. Meulenkaamp (2002) *Phys. Rev. Lett.* **89**, 036801.
- [49] J. Gilot, M. M. Wienk, R. A. J. Janssen (2007) *Appl. Phys. Lett.* **90**, 143512.
- [50] C. Lao, C. P. Wong, Z. L. Wang (2007) *Nano Lett.* **7**, 1323–1328.
- [51] S. K. Hau, H.-L. Yip, N. S. Baek, J. Zou, K. K. O'Malley, A. K. Y. Jen, (2007) *Appl. Phys. Lett.* **92**, 253301–1–253301–3.
- [52] Y. Sun, J. W. Seo, C. J. Takacs, J. Seifter, A. J. Heeger (2011) *Adv. Mater.* **23**, 1679–1683.
- [53] D. R. Bekci, A. Karsli, A. C. Cakir, H. Sarica, A. Guloglu, S. Gunes, S. Erten-Ela (2012) *Appl. Energy* **96**, 417–421.
- [54] C. Xu, G. Xu, Y. Liu, G. Wang (2002) *Solid State Commun.* **122**, 175–179.
- [55] W. U. Huynh, J. J. Dittmer, A. P. Alivisatos (2002) *Science* **295**, 2425–2427.
- [56] R. H. Friend, R. W. Gymer, A. B. Holmes, J. H. Burroughes, R. N. Marks, C. Taliani, D. D. C. Bradley, D. A. Dos Santos, J. L. Brédas, M. Lögdlund, W. R. Salaneck (1999) *Nature* **397**, 121–128.
- [57] B. C. Thompson, J. M. J. Fréchet (2007) *Angew. Chem., Int. Ed.* **47**, 58–77.
- [58] P. Herguth, X. Jiang, M. S. Liu, A. K. Y. Jen (2002) *Macromolecules* **35**, 6094–6100.

Acknowledgements

이번 겨울은 따뜻했던 우리 O.O.M lab 을 떠나려니 더 추운 겨울을 보낼 듯 합니다.

먼저, 제가 이 자리에 오기까지 어릴 적부터 보살펴 주신 사랑하는 우리 할머니, 아버지, 어머니, 고모들, 고모부들, 작은아버지들과 작은어머니들께 깊은 감사의 말씀 전합니다. 제가 더 많은 효도 할 수 있도록 오래오래 건강하세요. 사랑합니다. 그리고 늘 버팀목이 되어 준 사랑하는 왕언니 늘이 언니, 쌍둥이 예지 언니. 언니들~ 언제나 내 결정에 도움을 주고 응원해 줘서 고마워. 앞으로도 우리 세자매 지금처럼 예쁘게 잘 지내자.

김주현 교수님. 학부 시절부터 저에게 크나 큰 가르침을 주시고, 항상 예뻐해 주셔서 감사 합니다. 교수님 밑에 있으면서 많은 것을 배우고 덕분에 무사히 석사도 마칠 수 있게 되었습니다. 교수님 말씀처럼 항상 자부심은 갖지 말되 자신감을 갖는 겸손하고 당당한 엔지니어가 되겠습니다. 그리고 많은 가르침을 주신 민성기 교수님, 이봉 교수님, 박상보 교수님, 박찬영 교수님, 이원기 교수님, 유성일 교수님께도 깊은 감사의 말씀을 전합니다.

석사 생활을 함께해 온 우리 O.O.M lab 식구들. 많은 조언과 격려를 해주신 졸업하신 웅선배, 헤리언니, 상준선배, 정배선배, 선영언니, 준휘선배, 대성선배 감사합니다. 그리고 지금 까지도 저와 같이 생활하며 많이 가르쳐 주신 미영언니,

Trang 언니. 언니들이 있어서 더 많은 것을 보고 듣고 배울 수 있었던 것 같아요. 감사합니다. 그리고 부족한 저를 잘 따라와준 실험실 후배 종현선배, 경은이, 준환선배. 고맙습니다. 대학원 동기 순욱선배. 저 챙겨 주신다고 고생 많았어요. 둘 다 열심히 해서 우리 O.O.M 을 더 빛냅시다. 그리고 학사, 석사 6 년 동안 함께해온 내 친구 원민이. 늘 내편에서 응원하고 긍정의 에너지를 줘서 고마워.

그리고 나를 항상 최고로 알고 용기를 북돋아 주는 예쁜 내 친구들 지영, 준영, 정희. 너희가 있어서 난 무엇이든 다해낼 수 있는 천하장사가 된 듯해. 지금처럼 늘 잘 지내자. 대학 생활 중 내 일부였던 댄스동아리 네오쇼크 선배 후배 동기들. 나의 모델 해심선배, 정신적 지주 섹시담당 가영이. 늘 힘이 되고 즐거운 대학생활을 보낼 수 있게 해주셔서 감사합니다. 그리고 08 학번 보물 동기들. 효진, 유진, 은미, 정이, 정우, 슬기, 윤석, 지성, 준수오빠, 동효. 지금처럼 늘 웃으면서 잘 지내자.

그 외에도 제가 석사생활을 무사히 마칠 수 있게 도와주신 많은 분들께 감사드립니다. 더 열심히 해서 더 발전할 수 있는 사람이 되겠습니다.